

Flavor dependence of baryon melting temperature in effective models of QCD

Juan M. Torres-Rincon, Benjamin Sintès, and Joerg Aichelin

Subatech, UMR 6457, IN2P3/CNRS, Université de Nantes, École de Mines de Nantes, 4 Rue Alfred Kastler, F-44307 Nantes, France

(Received 16 February 2015; revised manuscript received 29 April 2015; published 25 June 2015)

We apply the three-flavor (Polyakov-)Nambu-Jona-Lasinio model to generate baryons as quark-diquark bound states using many-body techniques at finite temperature. All the baryonic states belonging to the octet and decuplet flavor representations are generated in the isospin-symmetric case. For each state we extract the melting temperature at which the baryon may decay into a quark-diquark pair. We seek for an evidence of the strangeness dependence of the baryon melting temperature as suggested by the statistical thermal models and supported by lattice quantum chromodynamics results. A clear and robust signal for this claim is found, pointing to a flavor dependence of the hadronic deconfinement temperature.

DOI: [10.1103/PhysRevC.91.065206](https://doi.org/10.1103/PhysRevC.91.065206)

PACS number(s): 11.10.Wx, 11.30.Rd, 11.10.St, 14.20.-c

I. INTRODUCTION

Experiments at the relativistic heavy-ion collider and the large hadron collider (LHC) have shown that a quark-gluon plasma (QGP) is produced during the first stages of a relativistic heavy-ion collision. The QGP is the phase of quantum chromodynamics (QCD) at high temperature or density where quarks and gluons are not color-confined into hadrons. From this QGP phase, the produced fireball undergoes a transition to the hadronic phase at a given hadronization temperature.

At nearly vanishing baryochemical potential the phase transition to the hadronic state is known to be a crossover [1]. Experimentally it is known that at the so-called chemical freeze-out temperature, which at vanishing chemical potential is close to the hadronization temperature, the hadrons are in statistical equilibrium. This is the result of a fit of the hadron abundances in the framework of a statistical model [2,3]. This fit determines the chemical freeze-out temperature and describes the multiplicity of almost all nonresonant hadrons with an astonishing precision. After chemical freeze-out the hadrons still interact but the chemical composition of the hadron gas remains (almost) unchanged. Results from high energetic central Pb + Pb collisions at LHC show that the freeze-out temperatures extracted by thermal fits [4] are close to the crossover temperature predicted by lattice-QCD studies [5].

A natural question to ask is whether the freeze-out conditions depend on the hadron species, i.e., if the chemical freeze-out temperature depends on flavor. Thermal fits presented in Ref. [4] show a tension when fitting the different baryonic species with a common freeze-out temperature, suggesting that the chemical freeze-out temperature for nonstrange baryons is smaller (around 16 MeV) than that for strange baryons [3,4]. In Refs. [6–8] it is shown that thermal fits with two independent freeze-out temperatures (for nonstrange and strange hadrons) provide a better description of the hadronic yields and considerably reduce the χ^2 (per degree of freedom) of the fit. This holds for a wide range of collision energies between $\sqrt{s_{NN}} = 6.27$ GeV and $\sqrt{s_{NN}} = 2.76$ TeV. In particular, for Pb + Pb collisions at LHC with $\sqrt{s_{NN}} = 2.76$ TeV the difference between the two freeze-out temperatures is around 15 MeV [6].

If this is the case, one may suggest that the hadronization temperature also depends on the strangeness content of the hadron. This idea was brought up quite recently by the authors of Ref. [9]. In this reference, the strangeness dependence of the crossover temperature was studied with continuum-extrapolated results of lattice-QCD calculations. The conclusion was that the crossover temperature (measured by the maximum of a susceptibility ratio) is about 15 MeV larger for strange hadrons than for those composed by light quarks. This difference is in surprisingly good accordance with the results from statistical-thermal fits of ALICE abundances, even if the two physical processes (hadronization and chemical freeze-out) are conceptually distinct.

In this paper we study the flavor dependence of the hadronization temperature by using one of the simplest effective models for strong interactions. The Nambu-Jona-Lasinio (NJL) model is an effective model for low-energy QCD where the gluonic fields are integrated out and the basic interaction consists of a four-quark contact vertex. Although the gluon dynamics is absent in this model, some of the gluonic features can be reproduced by the so-called Polyakov-Nambu-Jona-Lasinio (PNJL) model.

This effective model lacks true confinement. However, hadrons can be thought of as dynamically generated states from multi-quark rescattering, thus providing a nonperturbative mechanism for an effective confinement. The properties of these hadrons (masses and widths) can be obtained by solving the Bethe-Salpeter (BS) equation (for mesons) and the Fadeev equation (for baryons) with some approximations. Many approaches have been applied in which meson and baryon properties at zero temperature have been computed within the NJL and PNJL models [10–14]. These models can be extended to finite temperatures and densities. Such an extension allows for calculating the “Mott temperature,” the temperature at which hadrons are not bound anymore, because they can melt into a quark and a diquark.

Our aim is to find the Mott temperature for several hadrons within the three-flavor NJL and PNJL models, and extract conclusions about its dependence on the strangeness content of the hadrons. In Sec. II we introduce the NJL and PNJL Lagrangians and provide a short remainder on how a meson can be effectively described as a bound state of a quark-antiquark

pair. In Sec. III we use the Bethe-Salpeter equation for two quarks to generate diquarks and extract their properties as a function of the temperature. In Sec. IV we apply the Fadeev equation to generate baryons as bound states of quarks and diquarks. We will present the baryon masses as a function of temperature up to the melting (or Mott) temperature. We consider all baryons belonging to the octet and decuplet flavor representations in the isospin limit (up and down quarks with equal masses). Finally, in Sec. V we present our conclusions, summary, and outlook. We also include six appendixes with technical details, so keep this paper as much self-contained as possible: In Appendix A we detail the Fierz transformation for the NJL Lagrangian and discuss different versions found in the literature. Next, in Appendix B we shortly define the thermal functions needed in the calculation of the quark condensate and the meson or diquark polarization function. Appendix C is devoted to the simplification of the Bethe-Salpeter equation for diquarks and provide the flavor matrices for the different diquark sectors. In Appendix D we reduce the Fadeev equation for baryons to a tractable form using the “static approximation.” In Appendix E we present the projectors on the physical baryon states belonging to the octet and decuplet flavor representations. Finally, Appendix F is devoted to the simplification of the quark-diquark polarization function, providing useful expressions.

II. NAMBU-JONA-LASINIO MODEL FOR QUARKS

A. Effective Lagrangian

The NJL model [10,11,15,16] describes the low-energy interactions of quarks by a four-fermion contact vertex. Being an effective model of QCD it respects the symmetries of the underlying theory, in particular the $U_V(1) \otimes SU_V(N_f) \otimes SU_A(N_f)$ global symmetries of the massless QCD Lagrangian. The $U_V(1)$ symmetry leads to the baryon number conservation, while the chiral symmetry $SU_V(N_f) \otimes SU_A(N_f)$ is spontaneously broken down to $SU_V(N_f)$ at low temperatures. The $U_A(1)$ symmetry is broken by the axial anomaly.

The form of the NJL Lagrangian is motivated by QCD. Consider the quark-antiquark current-current scattering in the t channel, mediated by a dressed gluon. The gluon propagator gives a factor $1/(t - m_g^2)$, with m_g being the dressed gluon mass. In the limit of low momentum transfer one can neglect t in comparison with the gluon mass, thus producing an effective contact interaction among quarks. In this way, the gauge fields disappear from the theory and all what remains is an effective coupling g between quarks, related to the strong coupling constant and to the gluon mass.

For three flavors, the resulting effective interaction Lagrangian reads

$$\mathcal{L} = -g \sum_{a'} \sum_{ij} (\bar{\psi}_i \gamma^\mu T^{a'} \psi_i) (\bar{\psi}_j \gamma_\mu T^{a'} \psi_j), \quad (1)$$

where $i, j = 1, \dots, N_f = 3$ are flavor indices and $a' = 1, \dots, N_c^2 - 1$ are color indices with $T^{a'}$ being the color generators, which for $N_c = 3$ they are represented by the Gell-Mann matrices,

$$T^{a'} = \lambda^{a'}, \quad (2)$$

with the standard normalization,

$$\text{tr}_c (T^{a'} T^{b'}) = 2\delta^{a'b'}, \quad (3)$$

where tr_c denote the trace in color space.

After performing a Fierz transformation [10,11] this Lagrangian can be reexpressed in a convenient way to describe the $qq, \bar{q}\bar{q}$ and $\bar{q}q$ scattering. Using the Fierz transformation described in Appendix A we first obtain the $\bar{q}q$ sector of the effective theory, which will allow us to describe mesons. For instance, the pseudoscalar sector of the interacting Lagrangian (A4) reads (all repeated indices are to be summed)

$$\mathcal{L}_{\bar{q}q} = G (\bar{\psi}_i i\gamma_5 \tau_{ij}^a \psi_j) (\bar{\psi}_k i\gamma_5 \tau_{kl}^a \psi_l), \quad (4)$$

where $a = 1, \dots, N_f^2 - 1$ and G is a coupling constant, proportional to the original g in Eq. (1). In this work, we will take G as a free parameter to be fixed by comparing our results with the experimental hadron spectrum. The flavor generators τ^a follow the normalization,

$$\text{tr} (\tau^a \tau^b) = 2\delta^{ab}. \quad (5)$$

For $N_f = 3$ they can be represented by the Gell-Mann matrices.

The axial anomaly is responsible for the $U_A(1)$ breaking and gives rise to the observed $\eta - \eta'$ mass splitting. To account for this effect in the our model, we complement the NJL $\bar{q}q$ Lagrangian in Eq. (4) with the 't Hooft Lagrangian:

$$\mathcal{L}_H = -H \det_{ij} [\bar{\psi}_i (\mathbb{I} - \gamma_5) \psi_j] - H \det_{ij} [\bar{\psi}_i (\mathbb{I} + \gamma_5) \psi_j], \quad (6)$$

where H is an additional unknown coupling and \mathbb{I} is the identity matrix in Dirac space. For $N_f = 3$ this Lagrangian represents a six-point fermion interaction, which is effectively projected onto a four-fermion interaction by using the mean-field approximation [10,11]. Using the same approximation, the quark masses obey the gap equation,

$$m_i = m_{i0} - 4G \langle \bar{\psi}_i \psi_i \rangle + 2H \langle \bar{\psi}_j \psi_j \rangle \langle \bar{\psi}_k \psi_k \rangle, \quad j, k \neq i; j \neq k \quad (7)$$

with m_{i0} being the bare quark mass for flavor i , and the quark condensate defined as

$$\langle \bar{\psi}_i \psi_i \rangle = -i N_c \text{tr}_\gamma \int \frac{d^4 k}{(2\pi)^4} S_i(k), \quad (8)$$

with the trace acting in Dirac space. We represent by S_i the dressed quark propagator,

$$S_i(k) = \frac{1}{\not{k} - m_i}. \quad (9)$$

The final expression for the quark condensate in the NJL model is shown in Appendix B.

B. Medium effects

To calculate the hadron properties at finite temperature, we use the imaginary time formalism with the prescription,

$$\int \frac{d^4 k}{(2\pi)^4} \rightarrow iT \sum_{n \in \mathbb{Z}} \int \frac{d^3 k}{(2\pi)^3}, \quad (10)$$

with T the temperature and $k^0 \rightarrow i\omega_n$ the fermionic Matsubara frequencies $i\omega_n = i\pi T(2n+1)$.

To account for the finite baryonic density we can introduce a quark chemical potential by adding to the Lagrangian the term,

$$\mathcal{L}_\mu = \sum_{ij} \bar{\psi}_i \mu_{ij} \gamma_0 \psi_j, \quad (11)$$

where $\mu_{ij} = \text{diag}(\mu_u, \mu_d, \mu_s)$ contains the quark chemical potentials (which can be alternatively expressed in terms of the baryon, charge, and strangeness chemical potentials, μ_B, μ_Q, μ_S). In this work we will restrict ourselves to a vanishing chemical potential $\mu_u = \mu_d = \mu_s = 0$.

C. Polyakov-NJL model

In the NJL Lagrangian, the gluon fields have been integrated out of the fundamental theory. However, one can still introduce a source of gluonic effects through the Polyakov line,

$$L(\mathbf{x}) = \mathcal{P} \exp \left(i \int_0^\beta d\tau A_4(\tau, \mathbf{x}) \right), \quad (12)$$

where $\beta = 1/T$, \mathcal{P} is the path-ordering operator, and $A_4 = iA^0$ the temporal component of the gluon field in Euclidean space (with $A^\mu = g_s A_a^\mu T_a$). The order parameter of the deconfinement phase transition (in the absence of quarks) is chosen to be the Polyakov loop Φ , which is the thermal expectation value,

$$\Phi = \frac{1}{N_c} \text{tr}_c \langle L \rangle, \quad (13)$$

where the trace is taken in color space. To account for deconfinement effects via the Polyakov loop, an effective potential $\mathcal{U}(\Phi, \bar{\Phi}, T)$ is added to the effective NJL Lagrangian $\mathcal{L} \rightarrow \mathcal{L} - \mathcal{U}$. \mathcal{U} is a function of the Polyakov loop and its complex conjugate, which are taken to be homogeneous fields. The form of the effective potential is inspired by the \mathbb{Z}_3 center symmetry [17],

$$\frac{\mathcal{U}(T, \Phi, \bar{\Phi})}{T^4} = -\frac{b_2(T)}{2} \bar{\Phi} \Phi - \frac{b_3}{6} (\Phi^3 + \bar{\Phi}^3) + \frac{b_4}{4} (\bar{\Phi} \Phi)^2, \quad (14)$$

with

$$b_2(T) = a_0 + a_1 \frac{T_0}{T} + a_2 \left(\frac{T_0}{T} \right)^2 + a_3 \left(\frac{T_0}{T} \right)^3. \quad (15)$$

The parameters $a_0, a_1, a_2, a_3, b_3, b_4$, and T_0 are fitted from the pure-gauge lattice-QCD equation of state at zero chemical potential [17]. The numerical values of our parameters are given in Table I. Following the reasoning of Ref. [18] we have considered the running of T_0 with the number of flavors.

As a consequence, we have modified the original parameter $T_0 = 270$ MeV for the Yang-Mills case ($N_f = 0$) to a value of $T_0 = 190$ MeV for our case ($N_f = 2 + 1$).

This model is called the Polyakov-Nambu-Jona-Lasinio model and was widely used in similar studies as ours, e.g., for QCD thermodynamics [17] or generation of bound states [19–21].

The PNJL grand-canonical potential reads

$$\begin{aligned} \Omega_{\text{PNJL}}(\Phi, \bar{\Phi}, m_i, T) = & \mathcal{U}(T, \Phi, \bar{\Phi}) + 2G \sum_i \langle \bar{\psi}_i \psi_i \rangle^2 \\ & - 4H \prod_i \langle \bar{\psi}_i \psi_i \rangle - 2N_c \sum_i \int \frac{d^3k}{(2\pi)^3} E_i \\ & - 2T \sum_i \int \frac{d^3k}{(2\pi)^3} [\text{tr}_c \log(1 + L e^{-E_i/T}) \\ & + \text{tr}_c \log(1 + L^\dagger e^{-E_i/T})], \end{aligned} \quad (16)$$

with $E_i = \sqrt{k^2 + m_i^2}$. Using the mean-field approximation one has [19]

$$\begin{aligned} \text{tr}_c \log(1 + L e^{-E_i/T}) \\ = \log(1 + 3(\Phi + \bar{\Phi} e^{-E_i/T}) e^{-E_i/T} + e^{-3E_i/T}), \end{aligned} \quad (17)$$

$$\begin{aligned} \text{tr}_c \log(1 + L^\dagger e^{-E_i/T}) \\ = \log(1 + 3(\bar{\Phi} + \Phi e^{-E_i/T}) e^{-E_i/T} + e^{-3E_i/T}). \end{aligned} \quad (18)$$

We minimize the grand-canonical potential with respect to the order parameters: $\Phi, \bar{\Phi}, \langle \bar{\psi}_i \psi_i \rangle$,

$$\frac{\partial \Omega_{\text{PNJL}}}{\partial \Phi} = 0, \quad \frac{\partial \Omega_{\text{PNJL}}}{\partial \bar{\Phi}} = 0, \quad \frac{\partial \Omega_{\text{PNJL}}}{\partial \langle \bar{\psi}_i \psi_i \rangle} = 0. \quad (19)$$

The last equation provides the expression for the quark condensate in the PNJL model,

$$\langle \bar{\psi}_i \psi_i \rangle = -2N_c \int \frac{d^3k}{(2\pi)^3} \frac{m_i}{E_i} [1 - f_\Phi^+(E_i) - f_\Phi^-(E_i)], \quad (20)$$

with

$$f_\Phi^+(E_i) = \frac{(\Phi + 2\bar{\Phi} e^{-E_i/T}) e^{-E_i/T} + e^{-3E_i/T}}{1 + 3(\Phi + \bar{\Phi} e^{-E_i/T}) e^{-E_i/T} + e^{-3E_i/T}}, \quad (21)$$

$$f_\Phi^-(E_i) = \frac{(\bar{\Phi} + 2\Phi e^{-E_i/T}) e^{-E_i/T} + e^{-3E_i/T}}{1 + 3(\bar{\Phi} + \Phi e^{-E_i/T}) e^{-E_i/T} + e^{-3E_i/T}}. \quad (22)$$

For $N_f = 3$, the gap relation (7) and the first two equations in (19) form a system of five coupled equations. The system needs to be solved numerically to obtain the value of the Polyakov loop (and its conjugate) and the quark masses. In the isospin limit, two equations are degenerate giving $m_u = m_d$

TABLE I. Parameters of the NJL and PNJL model used in this study. In the isospin limit we have $m_{q0} = m_{u0} = m_{d0}$.

Parameter	m_{q0}	m_{s0}	Λ	G	H	G_{DIQ}	$G_{\text{DIQ},v}$
Value	5.5 MeV	134 MeV	569 MeV	$2.3/\Lambda^2$	$11/\Lambda^5$	$1.56 G$	$-0.639 G_{\text{DIQ}}$
Parameter	a_0	a_1	a_2	a_3	b_3	b_4	T_0
Value	6.75	-1.95	2.625	-7.44	0.75	7.5	190 MeV

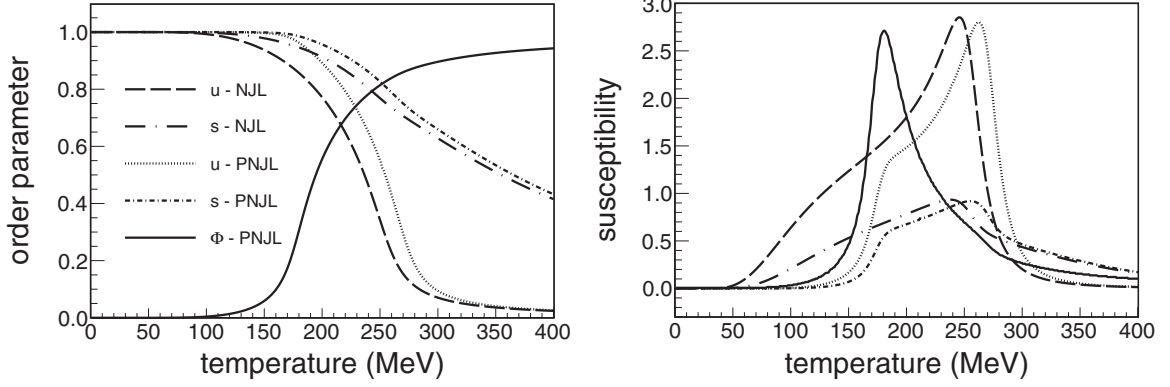


FIG. 1. (Left panel) Light and strange quark condensates (for both NJL and PNJL models) and Polyakov loop as a function of the temperature. In the legend, u and s stand for $\langle\bar{\psi}_u\psi_u\rangle(T)/\langle\bar{\psi}_u\psi_u\rangle(T=0)$ and $\langle\bar{\psi}_s\psi_s\rangle(T)/\langle\bar{\psi}_s\psi_s\rangle(T=0)$, respectively. (Right panel) Chiral and deconfinement susceptibilities as a function of temperature. Their maxima show the chiral and deconfinement transition temperatures. In this panel, the labels u, d , and Φ stand, respectively, for $\chi_{\langle\bar{\psi}_u\psi_u\rangle}(T)$, $\chi_{\langle\bar{\psi}_s\psi_s\rangle}(T)$, and $\chi_\Phi(T)$.

(and $\langle\bar{\psi}_u\psi_u\rangle = \langle\bar{\psi}_d\psi_d\rangle$). In addition, at vanishing chemical potential one has $\Phi = \bar{\Phi}$, which is evident from our equations.

In the left panel of Fig. 1 we show the temperature dependence of the light and strange quark condensates, $\langle\bar{\psi}_u\psi_u\rangle$ and $\langle\bar{\psi}_s\psi_s\rangle$, for both NJL and PNJL models. In addition, we also show the Polyakov loop as a function of T . These quantities serve as order parameters of the chiral and deconfinement phase transitions. The transition temperature can be defined as the point at which the susceptibility (derivative of the order parameter) peaks. In the right panel of Fig. 1 we plot the dimensionless chiral susceptibilities defined as

$$\chi_{\langle\bar{\psi}_u\psi_u\rangle} \equiv \frac{1}{T^2} \frac{d\langle\bar{\psi}_u\psi_u\rangle}{dT}, \quad \chi_{\langle\bar{\psi}_s\psi_s\rangle} \equiv \frac{1}{T^2} \frac{d\langle\bar{\psi}_s\psi_s\rangle}{dT}. \quad (23)$$

The maximum of the susceptibility will indicate the chiral transition temperature. They read $T_{\langle\bar{\psi}_u\psi_u\rangle} = 246/262$ MeV (NJL/PNJL) and $T_{\langle\bar{\psi}_s\psi_s\rangle} = 238/255$ MeV (NJL/PNJL). We also show the deconfinement susceptibility defined as

$$\chi_\Phi \equiv T \frac{d\Phi}{dT}, \quad (24)$$

whose maximum gives the approximate position of the deconfinement transition temperature $T_\Phi = 181$ MeV.

D. Mesons as bound states of $\bar{q}q$

To obtain the meson propagator one must solve the BS equation for the quark-antiquark scattering amplitude $i + \bar{j} \rightarrow m + \bar{n}$ (Latin subindices will denote quark flavor and barred indices antiquark flavor) in the random-phase approximation (RPA):

$$T_{i\bar{j},m\bar{n}}^{ab}(p^2) = \mathcal{K}_{i\bar{j},m\bar{n}}^{ab} + i \int \frac{d^4k}{(2\pi)^4} \mathcal{K}_{i\bar{j},p\bar{q}}^{ac} S_p\left(k + \frac{p}{2}\right) \times S_{\bar{q}}\left(k - \frac{p}{2}\right) T_{p\bar{q},m\bar{n}}^{cb}(p^2), \quad (25)$$

where a, b denotes the meson flavor channel. The kernel \mathcal{K} reads

$$\mathcal{K}_{i\bar{j},m\bar{n}}^{ab} = \Omega_{i\bar{j}}^a 2K^{ab} \bar{\Omega}_{\bar{n}m}^b, \quad (26)$$

with the vertex factors containing color, flavor, and spin matrices,

$$\Omega_{i\bar{j}}^a = (\mathbb{1}_{\text{color}} \otimes \tau_{i\bar{j}}^a \otimes \Gamma), \quad (27)$$

as well as a combinatorial factor of 2. The Dirac structure—whose indices we have omitted in our BS equation—can be chosen to be $\Gamma = \{1, i\gamma_5, \gamma^\mu, \gamma_5\gamma^\mu\}$ for scalar, pseudoscalar, vector, and axial-vector mesons, respectively.

The addition of the 't Hooft term to the NJL Lagrangian breaks flavor symmetry at the mean-field level of the coupling constants. The resulting flavor-dependent couplings in the $\bar{q}q$ sector K^{ab} are combinations of the G and H couplings [10]. In the pseudoscalar sector, the nonzero couplings read [10,22]

$$K^{00} = G + \frac{H}{3}(\langle\bar{\psi}_u\psi_u\rangle + \langle\bar{\psi}_d\psi_d\rangle + \langle\bar{\psi}_s\psi_s\rangle), \quad (28)$$

$$K^{11} = K^{22} = K^{33} = G - \frac{H}{2}\langle\bar{\psi}_s\psi_s\rangle, \quad (29)$$

$$K^{44} = K^{55} = G - \frac{H}{2}\langle\bar{\psi}_d\psi_d\rangle, \quad (30)$$

$$K^{66} = K^{77} = G - \frac{H}{2}\langle\bar{\psi}_u\psi_u\rangle, \quad (31)$$

$$K^{88} = G - \frac{H}{6}(2\langle\bar{\psi}_u\psi_u\rangle + 2\langle\bar{\psi}_d\psi_d\rangle - \langle\bar{\psi}_s\psi_s\rangle), \quad (32)$$

$$K^{03} = K^{30} = \frac{H}{2\sqrt{6}}(\langle\bar{\psi}_u\psi_u\rangle - \langle\bar{\psi}_d\psi_d\rangle), \quad (33)$$

$$K^{08} = K^{80} = \frac{-H}{2\sqrt{6}}(\langle\bar{\psi}_u\psi_u\rangle + \langle\bar{\psi}_d\psi_d\rangle - 2\langle\bar{\psi}_s\psi_s\rangle), \quad (34)$$

$$K^{38} = K^{83} = -\frac{H}{2\sqrt{3}}(\langle\bar{\psi}_u\psi_u\rangle - \langle\bar{\psi}_d\psi_d\rangle). \quad (35)$$

Notice that they are diagonal in flavor space except for the (0-3-8) subsystem. These nondiagonal couplings will eventually bring a $\pi^0 - \eta^0 - \eta^8$ mixing [10], which should be solved in the coupled-channel basis. In the isospin limit ($m_u = m_d$) the π^0 is decoupled from the system, but mixing is still present in the $\eta^0 - \eta^8$ subspace. In a diagonal basis, this fact accounts for the $\eta - \eta'$ mixing, providing the mass splitting between

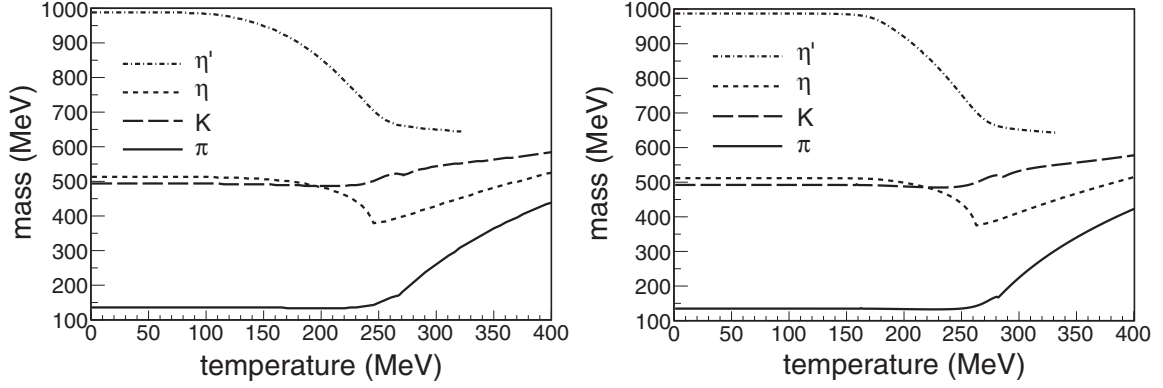


FIG. 2. Pseudoscalar meson masses as a function of the temperature for vanishing chemical potential in the NJL (left panel) and PNJL (right panel) models.

these two states. Note that in the absence of the 't Hooft term, the mixing disappears.

Introducing the function $t^{ab}(p^2)$,

$$T_{ij,m\bar{n}}^{ab}(p^2) = \Omega_{ij}^a t^{ab}(p^2) \bar{\Omega}_{\bar{n}m}^b, \quad (36)$$

the solution of the BS equation is a matrix in flavor space,

$$t^{ab}(p^2) = \left[\frac{2K}{1 - 2K\Pi(p^2)} \right]^{ab}, \quad (37)$$

where the polarization function $\Pi^{ab}(p^2)$ is defined as

$$\Pi^{ab}(p^2) = i \int \frac{d^4k}{(2\pi)^4} \text{tr}_\gamma \left[\bar{\Omega}_{ji}^a S_i \left(k + \frac{p}{2} \right) \Omega_{ij}^b S_j \left(k - \frac{p}{2} \right) \right]. \quad (38)$$

In Appendix B we provide a simplified expression for this function at finite temperature.

The poles of $t^{ab}(p^2)$ represent the mesonic states, which are bound states of the $\bar{q}q$ scattering. One can perform a Taylor expansion of the function $t^{-1,ab}(p^2)$ around the pole $p^2 = m_M^2$,

$$t^{-1,ab}(p^2) = t^{-1,ab}(m_M^2) + \left. \frac{\partial t^{-1,ab}(p^2)}{\partial p^2} \right|_{p^2=m_M^2} (p^2 - m_M^2) + \dots \simeq -\frac{1}{2m_M} \left. \frac{\partial \Pi^{ab}(p^2)}{\partial p} \right|_{p^2=m_M^2} (p^2 - m_M^2), \quad (39)$$

where we have used that $t^{-1,ab}(m_M^2) = 0$ at the pole position. Defining the effective coupling,

$$g_{M \rightarrow \bar{q}q}^2 \equiv \frac{2m_M}{\left. \frac{\partial \Pi^{ab}(p^2)}{\partial p} \right|_{p^2=m_M^2}}, \quad (40)$$

we show that $t^{ab}(p^2)$ can be identified with the meson propagator,

$$t^{ab}(p^2) = \frac{-g_{M \rightarrow \bar{q}q}^2}{p^2 - m_M^2}. \quad (41)$$

Therefore, the equation,

$$1 - 2K^{ab}\Pi^{ab}(p^2 = m_M^2) = 0, \quad (42)$$

gives the meson mass m_M in the appropriate flavor channel (and spin channel by selecting Γ).

If the generated state has a m_M larger than the sum of quarks masses, it is possible for this meson to decay into a quark-antiquark pair. In this case the polarization function (38) becomes complex and the pole acquires an imaginary part. Considering the variable p^2 as complex one can identify the mass and the decay width with the real and imaginary parts of the pole position. In this way one can obtain the meson masses and decay widths as a function of temperature and/or chemical potential. A detailed discussion about this procedure is provided at the end of Appendix B.

The parameters we use in this work are partially based on the findings of Ref. [23]. For the NJL model in the isospin limit we have seven parameters. The extension to the PNJL model introduces another seven parameters (fixed from the thermodynamics of pure-gauge QCD in the lattice [17]). All of them are summarized in Table I.

Using the parameter set in Table I we obtain the following at $T = 0$: the light-quark condensate $\langle \bar{\psi}_u \psi_u \rangle = -(241.3 \text{ MeV})^3$, the pion decay constant $f_\pi = 92.2 \text{ MeV}$, the pion mass $m_\pi = 134.8 \text{ MeV}$, the kaon mass $m_K = 492.1 \text{ MeV}$, the $\eta - \eta'$ mass splitting of 475.5 MeV, the proton mass 932.0 MeV, and the Δ baryon mass 1221.4 MeV.

Our results for pseudoscalar and vector meson masses are summarized in Figs. 2 and 3, respectively, where we include the results from both the NJL and the PNJL models.

In Table II we present the masses of the pseudoscalar and vector mesons at zero temperature, as well as the Mott temperatures for all of them, defined as the temperature at which

$$m_M(T_{\text{Mott}}) = m_p(T_{\text{Mott}}) + m_{\bar{q}}(T_{\text{Mott}}), \quad (43)$$

with m_p and $m_{\bar{q}}$ the masses of the quark and antiquark that compose the meson.

Notice that for each mesonic state a different Mott temperature is found; note also the large difference between the Mott temperatures within the NJL and the PNJL models. Given the uncertainties of our model one could argue that a common

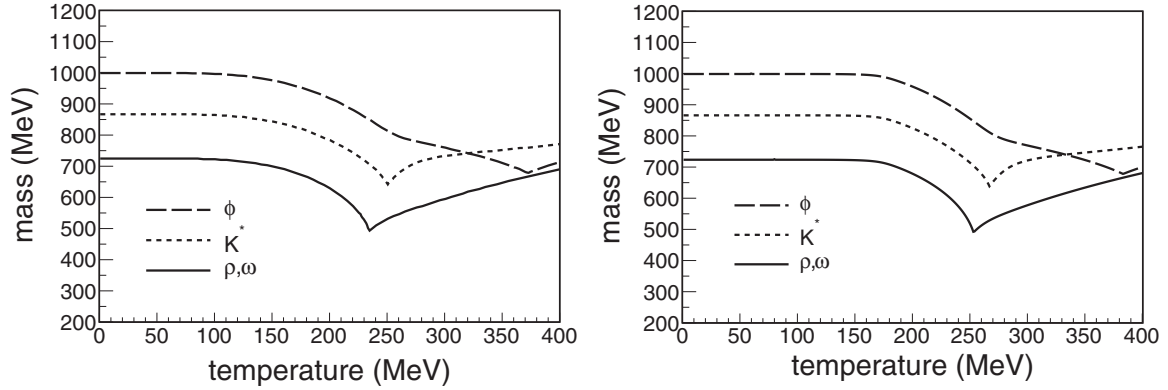


FIG. 3. Vector meson masses as a function of the temperature for vanishing chemical potential in the NJL (left panel) and PNJL (right panel) models.

Mott temperature may work for them all. Alternatively one might claim that more precise data are necessary to establish an eventual difference of the Mott temperature of pions and kaons, for instance. However, note that the ϕ meson has a very large Mott temperature, not consistent with the rest. This fact makes the ϕ meson impossible to accommodate in a global picture of common hadronization conditions. This would manifest itself in a larger ϕ/π ratio than the expected for a production at a common temperature, as seen experimentally in Ref. [25].

III. DIQUARKS

A second Fierz transformation can convert the original NJL interaction into Lagrangian that describes the interaction among quarks [11]. Their bound states, diquarks, belong to a nonsinglet color representation and are not experimentally observable states. However, they will be important for the construction of baryons.

It is important to fix the different diquark channels we consider. In color space, we neglect the sextet representation ($\mathbf{3}_c \otimes \mathbf{3}_c = \bar{\mathbf{3}}_c \oplus \mathbf{6}_c$) because the members of this representation cannot be combined with an additional quark to form colorless baryons (in addition, this channel is known to be repulsive). In flavor space, diquarks from both $\bar{\mathbf{3}}_f$ and $\mathbf{6}_f$ representations can take part in the baryon structure, but they should be appropriately combined with the spin structure to have a total antisymmetric wave function [14,26]. A summary of the different allowed channels is shown in Table III. All the allowed combinations can be alternatively obtained by applying a Fierz transformation to the original color-current

TABLE II. Masses at $T = 0$ and Mott temperatures for the pseudoscalar and vector mesons in the NJL and PNJL models. For the η' meson we find a finite decay width already at $T = 0$. All units are given in MeV.

Meson	π	K	η	η'	ρ	K^*	ω	ϕ
Mass at $T = 0$	135	492	512	987	723	866	723	998
Mass (PDG [24])	136	495	548	958	775	892	782	1020
T_{Mott} (NJL)	267	271	245	0	234	250	234	372
T_{Mott} (PNJL)	282	286	262	0	253	266	253	382

Lagrangian into the qq sector [11]. All the terms emerging from the Fierz transformation, exactly match all the different terms shown in Table III (see further discussion and final Lagrangian in Appendix A).

As we will see later, only the low-lying diquarks of each spin (scalar and axial-vector ones) will be used to form baryons. This is so because of the fact that the masses of the pseudoscalar and vector diquarks will be higher than the experimental baryon masses and already unstable at zero temperature. For this reason we only detail here the Lagrangian describing the scalar diquark sector,

$$\mathcal{L}_{qq} = G_{\text{DIQ}} (\bar{\psi} i \gamma_5 C \tau^A T^A \bar{\psi}^T) (\psi^T C i \gamma_5 \tau^A T^A \psi), \quad (44)$$

and the one for the axial diquark sector,

$$\mathcal{L}_{qq} = G_{\text{DIQ},V} (\bar{\psi} \gamma^\mu C \tau^S T^A \bar{\psi}^T) (\psi^T C \gamma_\mu \tau^S T^A \psi), \quad (45)$$

where G_{DIQ} and $G_{\text{DIQ},V}$ are coupling constants (related to the original g but taken here as free parameters) and $C = i \gamma_0 \gamma_2$ represents the charge-conjugation operation. Finally, we have denoted by τ^A and τ^S the antisymmetric and symmetric flavor matrices, respectively, and by T^A the antisymmetric color matrices. In particular, the presence of the latter reflects that the diquarks cannot be color singlets.

The BS equation for the quark-quark scattering in the RPA approximation reads

$$T_{ij,mn}^{ab}(p^2) = \mathcal{K}_{ij,mn}^{ab} + i \int \frac{d^4 k}{(2\pi)^4} \mathcal{K}_{ij,pq}^{ac} S_p \left(k + \frac{p}{2} \right) \times S_q \left(\frac{p}{2} - k \right) T_{pq,mn}^{cb}(p^2), \quad (46)$$

TABLE III. Different diquarks belonging to different sectors. Γ denotes the spin structure associated with the qq vertex.

Color	Flavor	J^P	Γ	Denomination
$\mathbf{6}_S$	Not considered here			
$\bar{\mathbf{3}}_A$	$\mathbf{6}_S$	1^+	γ_μ	Axial
$\bar{\mathbf{3}}_A$	$\bar{\mathbf{3}}_A$	0^+	$i \gamma_5$	Scalar
$\bar{\mathbf{3}}_A$	$\bar{\mathbf{3}}_A$	0^-	\mathbb{I}	Pseudoscalar
$\bar{\mathbf{3}}_A$	$\bar{\mathbf{3}}_A$	1^-	$\gamma_\mu \gamma_5$	Vector

where $S^c(p) \equiv C^{-1}S^T(-p)C$ denotes the charge-conjugated quark propagator, with T the transposed operator (not to be confused with the temperature).

Details concerning the simplification of this equation are given in Appendix C. In terms of the function $t^{ab}(p^2)$,

$$T_{ij,mn}^{ab}(p^2) = \Omega_{ij}^a t^{ab}(p^2) \bar{\Omega}_{nm}^b, \quad (47)$$

we can express the solution of the BS equation as

$$t^{ab}(p^2) = \frac{2G_{\text{DIQ}}}{1 - 2G_{\text{DIQ}}\Pi^{ab}(p^2)}, \quad (48)$$

with the quark-quark polarization function of Eq. (C6).

For the spin-1 channels the polarization function contains a transverse term and a longitudinal term,

$$\Pi_{\mu\nu}^{ab} = \Pi_{\perp}^{ab}\mathcal{T}_{\mu\nu} + \Pi_{\parallel}^{ab}\mathcal{L}_{\mu\nu}, \quad (49)$$

where we have defined the projectors,

$$\mathcal{T}_{\mu\nu} = g_{\mu\nu} - \frac{p_{\mu}p_{\nu}}{p^2}, \quad \mathcal{L}_{\mu\nu} = \frac{p_{\mu}p_{\nu}}{p^2}. \quad (50)$$

The solution of the spin-1 diquark masses involves the transverse component of the polarization function $\Pi_{\perp}^{ab}(p^2) = \frac{1}{3}\mathcal{T}^{\mu\nu}\Pi_{\mu\nu}^{ab}$. For axial diquarks this fact directly comes from the vector current conservation, but for vector diquarks this result still holds [27].

The function $t^{ab}(p^2)$ reads

$$t^{ab}(p^2) = \left[\frac{2G_{\text{DIQ},V}}{1 - 2G_{\text{DIQ},V}\Pi_{\perp}(p^2)} \right]^{ab}, \quad (51)$$

where the coupling constant $G_{\text{DIQ},V}$ for vector and axial diquarks is, in principle, related to G_{DIQ} by the Fierz transformation. However, we will take it here as a free parameter to be fixed by a fit to the baryon masses.

Again, the poles of the $t^{ab}(p^2)$ functions are identified with dynamically generated diquarks in their respective flavor and spin channel. The diquark mass, m_{DIQ} , is obtained by the solution of the equations $1 - 2G_{\text{DIQ}}\Pi^{ab}(m_{\text{DIQ}}^2) = 0$ for spin zero diquarks and $1 - 2G_{\text{DIQ},V}\Pi_{\perp}^{ab}(m_{\text{DIQ}}^2) = 0$ for spin one diquarks.

In Fig. 4 we present our results for scalar and axial diquark masses, which will be used to model baryons in the next section. Scalar diquarks are represented by square brackets $[q_1q_2]$ and axial diquarks by parenthesis (q_1q_2) . From Fig. 4 it is possible to read off the Mott temperature for the different states (defined as the temperature at which the mass of the bound state equals the sum of the quark masses). Beyond this temperature, a diquark thermal width is generated, which represents the probability of the diquark to decay into a pair of quarks.

For completeness, we also present our results for the pseudoscalar $\{q_1q_2\}$ and vector $\langle q_1q_2 \rangle$ diquarks in Fig. 5. As we have anticipated, at $T = 0$ these states have a finite thermal decay width which excludes a role in forming stable baryons at low temperatures. For this reason, we will neglect these states hereafter.

We now turn to the PNJL model and show the results for the scalar and axial diquark masses with the parameter set presented in Table I. In Fig. 6 we show the diquark masses

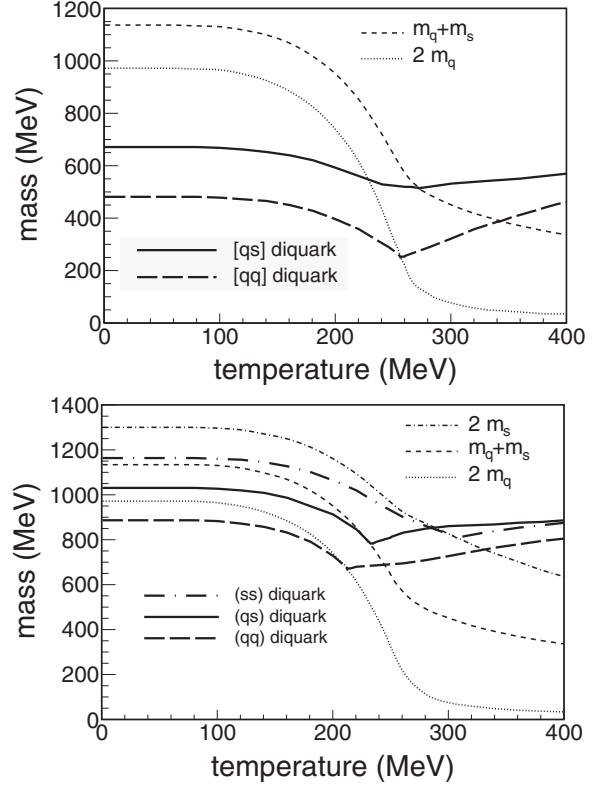


FIG. 4. Scalar diquark (upper panel) and axial diquark (lower panel) masses as a function of the temperature for vanishing chemical potential in the NJL model. For comparison, the thermal quark masses are also shown. q stands for light quark ($q = u = d$).

as a function of temperature at zero chemical potential. In this case, the quark masses are more stable as a function of the temperature, generating a systematically larger Mott temperature in comparison with the NJL model. At $T = 0$ the masses obtained from the NJL and PNJL models coincide, providing a consistency check.

In Table IV we present a summary of Mott temperatures (with precision of 1 MeV) for the different states in the NJL and in the PNJL model. The PNJL model shows higher melting temperatures in all cases. From this table one already sees a hint for the flavor dependence of the hadronization (Mott) temperature. This temperature increases with the strangeness content of the diquark.

Assuming the pole dominance of the diquark propagation, we can expand the $t^{ab}(p^2)$ function around its pole to obtain [11]

$$t^{ab}(p^2) = -\frac{g_{[qq] \rightarrow qq}^2}{p^2 - m_{\text{DIQ}}^2}. \quad (52)$$

Taking the diquark to be at rest ($\mathbf{p} = 0$) the effective coupling $g_{[q_1q_2] \rightarrow q_1q_2}^2$ is defined as

$$g_{[q_1q_2] \rightarrow q_1q_2}^2 = \frac{2m_{\text{DIQ}}}{\left. \frac{\partial \Pi^{ab}(p_0)}{\partial p_0} \right|_{p_0=m_{\text{DIQ}}}}. \quad (53)$$

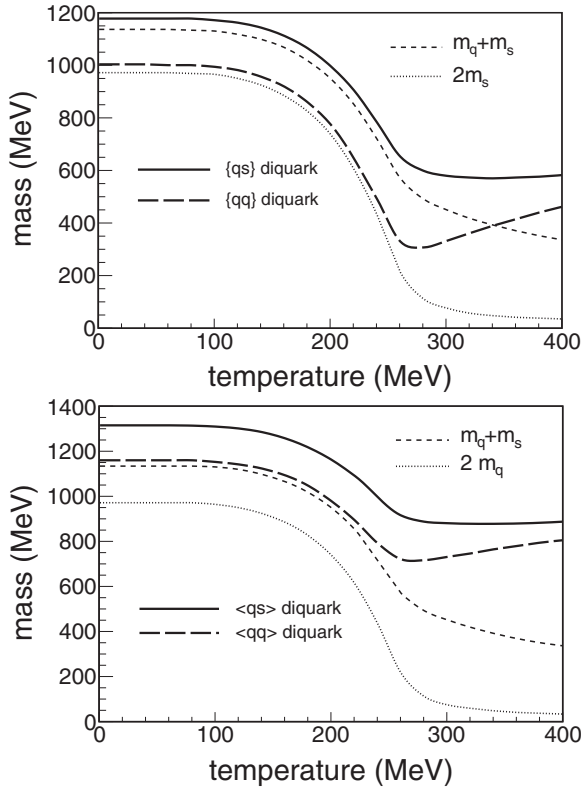


FIG. 5. Pseudoscalar diquark (upper panel) and vector diquark (lower panel) masses as a function of temperature for vanishing chemical potential in the NJL model. Notice that the diquark masses are always higher than the combined mass of their constituents. Therefore, they are unstable against decay to two quarks.

For the axial diquarks we find in the pole approximation,

$$t^{ab,\mu\nu}(p_0,0) = \frac{g_{(q_1q_2) \rightarrow q_1q_2}^2}{p_0^2 - m_{\text{DIQ}}^2} \left(g^{\mu\nu} - \frac{p^\mu p^\nu}{m_{\text{DIQ}}^2} \right), \quad (54)$$

with

$$g_{(q_1q_2) \rightarrow q_1q_2}^2 = \frac{-2m_{\text{DIQ}}}{\left. \frac{\partial \Pi_{\pm}^{ab}(p_0)}{\partial p_0} \right|_{p_0=m_{\text{DIQ}}}}. \quad (55)$$

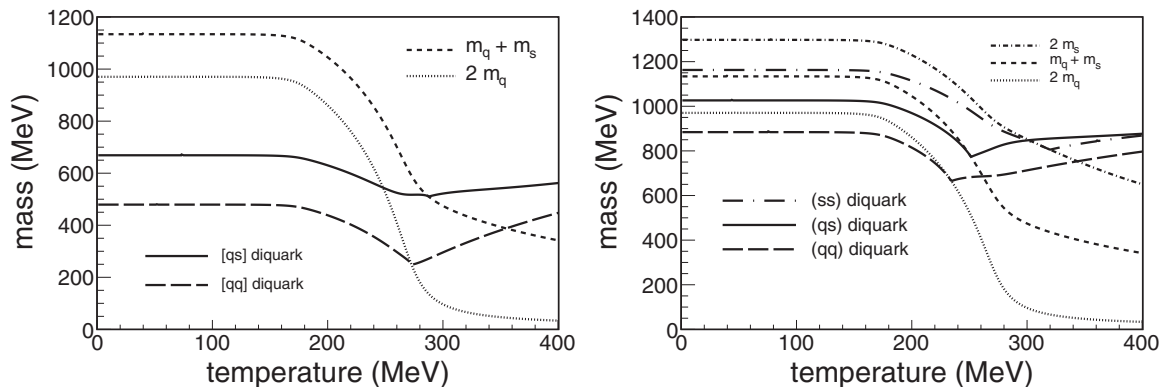


FIG. 6. Scalar diquark (left panel) and axial diquark (right panel) masses as a function of temperature for vanishing chemical potential in the PNJL model.

TABLE IV. Mott (or melting) temperature for the different scalar $[q_1q_2]$ and vector axial (q_1q_2) diquarks in the NJL as well as in the PNJL model.

Diquark	NJL T_{Mott} (MeV)	PNJL T_{Mott} (MeV)
$[qq]$	256	272
$[qs]$	273	287
(qq)	212	234
(qs)	233	251
(ss)	307	319

We now present our results for the effective couplings of the scalar and axial diquarks as a function of the temperature at vanishing chemical potential. The NJL results are given in Fig. 7 and those for the PNJL model in Fig. 8. Notice that the Mott temperature clearly coincides in these plots with the value at which the effective coupling vanishes.

IV. QUARK-DIQUARK BOUND STATES

In the last two sections we have explored the concept of “hadronization” as a dynamical generation of bound states from quark and antiquark scattering. This idea—quite successful for the generation of mesons and diquarks—can be pushed forward to describe baryons as bound states of a quark and a diquark. For $N_f = 3$ we will consider both the octet and decuplet flavor representations of baryons. Scalar diquarks (those belonging to flavor $\bar{\mathbf{3}}$ representation) and axial diquarks ($\mathbf{6}$) will be used to build up the baryon octet and decuplet states, respectively, according to the decomposition,

$$\mathbf{3} \otimes (\bar{\mathbf{3}} \oplus \mathbf{6}) = (\mathbf{1} \oplus \mathbf{8}) \oplus (\mathbf{8} \oplus \mathbf{10}). \quad (56)$$

Notice that the members of the octet also contain nonzero contribution from the axial diquarks. However, previous results at zero temperature have shown that the contribution is almost negligible [12]. For simplicity, we will neglect the axial diquark contribution to the baryon octet.

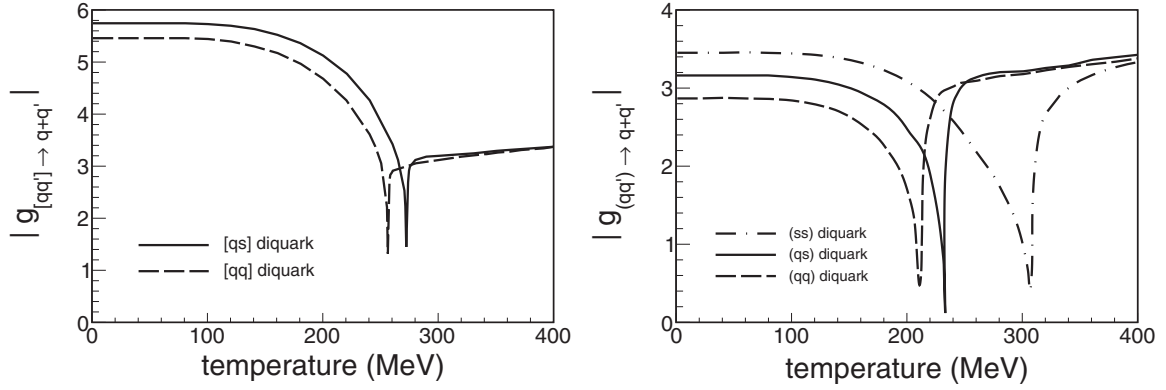


FIG. 7. Effective diquark-quark-quark coupling, defined in Eq. (53) for the scalar diquarks (left panel) and in Eq. (55) for the axial diquark (right panel) as a function of temperature in the NJL model.

The starting point to describe baryons is the Fadeev equation [13,28]:

$$X_j^{\bar{j},\alpha}(P^2, q) - \int \frac{d^4 k}{(2\pi)^4} L_{jk}^{\bar{j},\alpha\beta}(P^2, q, k) X_k^{\bar{k},\beta}(P^2, k) \Big|_{P^2=M_B^2} = 0, \quad (57)$$

where the baryon wave function is denoted by $X_j^{\bar{j},\alpha}$ and it carries a quark index (j), diquark index (\bar{j}), and a possible spin index α .

The kernel reads [13]

$$L_{jk}^{\bar{j},\alpha\beta}(P^2, q, k) = \mathcal{G}_{kk}^{\gamma\beta}(P^2, q) Z_{jk}^{\bar{k},\alpha\gamma}(q, k), \quad (58)$$

with a first term which accounts for the free quark and diquark propagators (see right panel of Fig. 9),

$$\mathcal{G}_{kk}^{\gamma\beta}(P^2, q) = S_k(P/2 + q) i t_k^{\gamma\beta}(P/2 - q), \quad (59)$$

and a second term,

$$Z_{jk}^{\bar{k},\alpha\gamma}(q, k) = \Omega_{jl}^{\bar{k},\gamma} S_l(-q - k) \Omega_{lk}^{\bar{j},\alpha}, \quad (60)$$

which represents an interaction with an exchanged quark (displayed in the left panel of Fig. 9).

We do not attempt here to justify the form of the Fadeev equation (57) and we refer the reader to the original papers [13,26] to learn the rigorous derivation and know more details.

Nevertheless, we can provide a simple motivation for Eq. (57): If we denote by $\mathbf{G}(P^2)$ the full baryon propagator, one can form a Dyson equation by taking \mathcal{G} as the leading order approximation (free propagation), and then considering Z as the elementary interaction (see Fig. 10).

The Dyson equation can be symbolically written as

$$\mathbf{G} = \mathcal{G} + \mathcal{G}Z\mathbf{G}, \quad (61)$$

whose solution reads

$$\mathbf{G} = \frac{\mathcal{G}}{1 - \mathcal{G}Z}. \quad (62)$$

The baryon masses are now extracted as the poles of the baryon propagator, so one needs to solve $\mathbf{G}^{-1}X(P^2 = M_B^2) = 0$, where X is the baryon wave function. Explicitly,

$$(1 - \mathcal{G}Z)X(P^2 = M_B^2) = 0, \quad (63)$$

at $P^2 = M_B^2$, which is a simplified version of the more complete Eq. (57).

The technical simplification of the Fadeev equation is given in Appendix D. There, we apply the ‘‘static approximation’’ for the exchanged quark [13]. This amounts to neglecting the

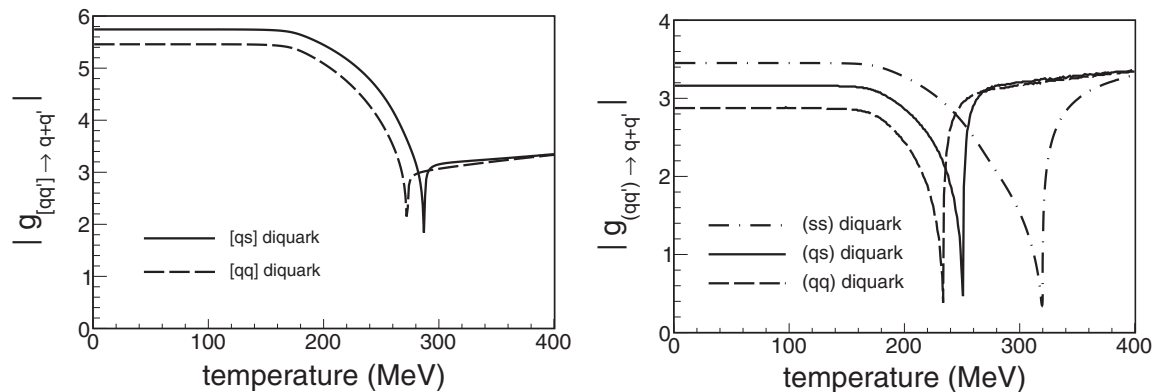


FIG. 8. Same as Fig. 7 but for the PNJL model.

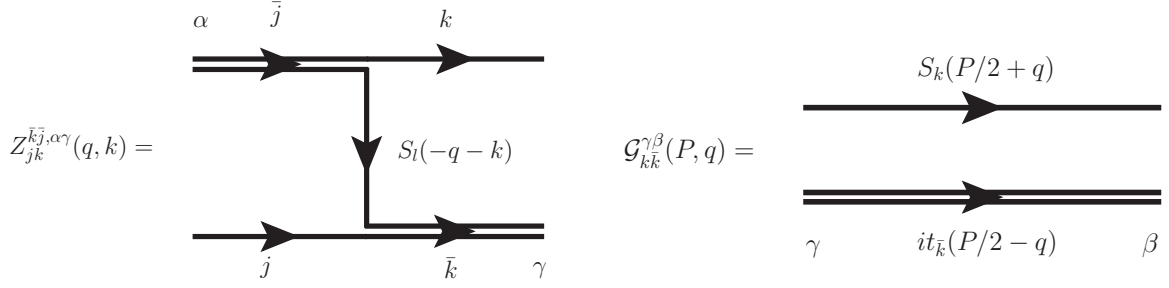


FIG. 9. (Left panel) Effective coupling in the Fadeev equation which contains a quark exchange. (Right panel) Two-particle (quark+diquark) propagator in the Fadeev kernel.

exchanged momentum in Z with respect to the quark mass m_l . This approximation was intensively used in other works resulting a very good approximation (the estimated uncertainty is around 5% as quoted in [13]).

As shown in Appendix D the Fadeev equation can be recasted into a Dirac-like equation for the baryon wave function evaluated at the baryon mass. For a particular baryon channel BB' (we denote by B, B' the physical baryon in the initial and final state), the equation to be solved reads

$$[g^{\alpha\beta} \delta^{BB'} - M^{BB', \alpha\beta}(P^2)]|_{P^2=m_B^2} = 0, \quad (64)$$

with the matrix (in both flavor and spin spaces) $M^{BB', \alpha\beta}$ introduced in Eq. (D7),

$$M^{BB', \alpha\beta}(P) \equiv \frac{2}{m_l} \int \frac{d^4 q}{(2\pi)^4} \mathcal{P}_{jj}^{\dagger, B} \mathcal{P}_{kk}^{B'} \tau_{jl}^{\bar{k}} \tau_{lk}^{\bar{j}} \Gamma^\mu \Gamma_\mu \times S_k\left(\frac{P}{2} + q\right) i t_k^{\alpha\beta}\left(\frac{P}{2} - q\right). \quad (65)$$

For the members of the baryon octet, $M^{BB'}$ simplifies to (D9)

$$M^{BB'}(P) = \frac{2}{m_l} \mathcal{P}_{jj}^{\dagger, B} \mathcal{P}_{kk}^{B'} \tau_{jl}^{\bar{k}} \tau_{lk}^{\bar{j}} \Pi_{k\bar{k}}(P), \quad (66)$$

where the flavor matrices τ are given on the top of Table VI, the projection matrices \mathcal{P} are given in Appendix E, and the quark-diquark polarization function is defined as

$$\Pi_{k\bar{k}}(P) \equiv - \int \frac{d^4 q}{(2\pi)^4} S_k(P - q) i t_k(q). \quad (67)$$

For the baryon decuplet the matrix $M^{BB', \alpha\beta}$ reads (D11)

$$M^{BB', \alpha\beta} = \frac{8}{m_l} \mathcal{P}_{jj}^{\dagger, B} \mathcal{P}_{kk}^{B'} \tau_{jl}^{\bar{k}} \tau_{lk}^{\bar{j}} \Pi_{k\bar{k}}^{\alpha\beta}(P), \quad (68)$$

where the flavor matrices for axial diquarks are given in the bottom of Table VI and the projection matrices are also given in Appendix E. The quark-diquark polarization function is

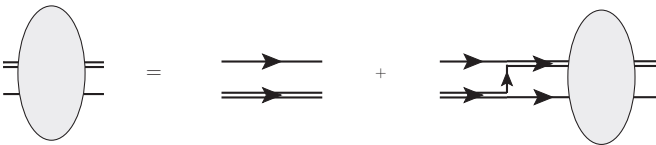


FIG. 10. Dyson equation for the baryon propagator $\mathbf{G} = \mathcal{G} + \mathcal{G}Z\mathbf{G}$.

defined as

$$\Pi_{k\bar{k}}^{\alpha\beta}(P) \equiv \int \frac{d^4 q}{(2\pi)^4} S_k(P - q) i t_k^{\alpha\beta}(q), \quad (69)$$

where its final expression is given in Appendix F.

In summary, the baryon masses are obtained by solving Eq. (64) with the matrix $M^{BB'}$ defined in (66) for the members of the baryon octet and in (68) for the members of the decuplet. The results for the masses and the extraction of the melting temperature for the different states are given in the next section.

V. RESULTS AND CONCLUSIONS

Our results for the baryon masses at finite temperature in both the octet and decuplet representations are shown in Fig. 11

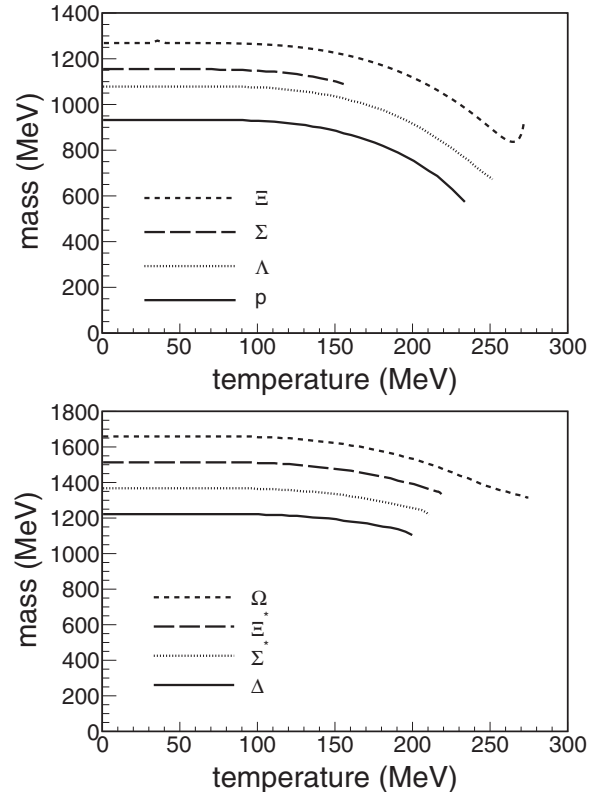


FIG. 11. Baryon masses as a function of temperature for vanishing chemical potential in the NJL model.

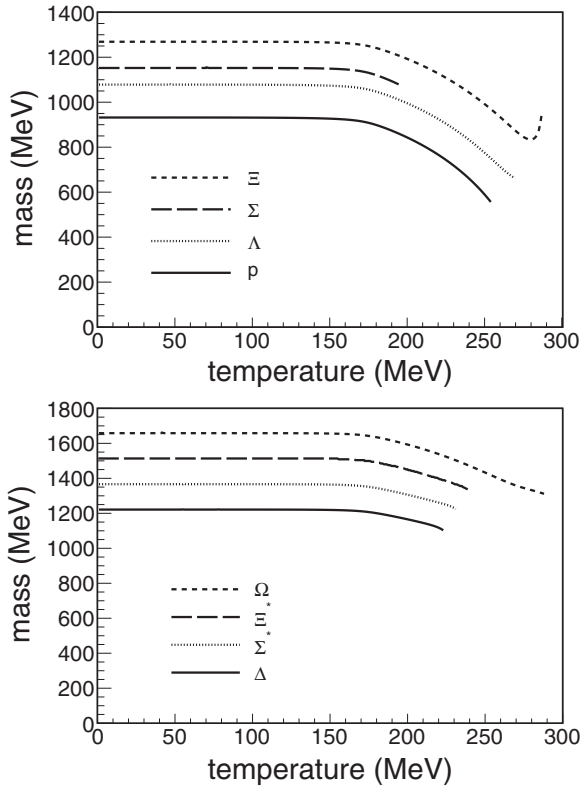


FIG. 12. Baryon masses as a function of temperature for vanishing chemical potential in the PNJL model.

for the NJL model. The results using the PNJL model are presented in Fig. 12. We summarized all the baryon masses in vacuum ($T = 0$) in Table V.

The masses are given as a function of temperature for vanishing chemical potential. As baryons are considered as quark-diquark bound states, the definition of the deconfinement temperature is slightly modified to take into account the possibility of diquark melting. The “deconfinement” temperature may be a genuine Mott temperature $T_{\text{Mott}}(\text{baryon})$, i.e., when the baryon mass equals the sum of quark and diquark masses. Nevertheless, it can also happen that the diquark melts at a lower temperature $T_{\text{Mott}}(\text{diquark}) < T_{\text{Mott}}(\text{baryon})$. Therefore, we define the baryon deconfinement temperature as the minimum of the two:

$$T_d \equiv \min\{T_{\text{Mott}}(\text{baryon}), T_{\text{Mott}}(\text{diquark})\}, \quad (70)$$

TABLE V. Masses at $T = 0$ and Mott temperature for the different baryons in the octet and decuplet representations for both NJL and PNJL models. All units are given in MeV.

Baryon	p	Λ	Σ	Ξ	Δ	Σ^*	Ξ^*	Ω
Mass at $T = 0$	932	1078	1152	1269	1221	1366	1512	1658
Mass (PDG) [24]	939	1116	1193	1318	1232	1383	1533	1672
T_{Mott} (NJL)	234	252	156	272	200	211	219	275
T_{Mott} (PNJL)	254	269	195	287	223	231	239	288

excluding the possibility that the three-quark system is stable when the diquark becomes unstable.

Baryon masses are plotted up to this temperature, which is summarized in Table V for all the baryon states. Beyond T_d the baryon mass becomes complex and, in principle, one should perform an analytical continuation of the Matsubara frequencies to nonreal energies. This is beyond the scope of this work.

Comparison with previous results [21,29–31] show a similar trend for all the masses. In particular the surprisingly low melting temperature for Σ baryon is also captured by [29,30] where, in addition, the melting temperature of proton is slightly larger than the Λ , as opposed to our case. In Refs. [21,31] the decuplet is shown for the first time. However, in these works the Dirac structure of the Dirac equation (D7) is simplified by taking the trace in the quark-diquark polarization function (with no further justification for this step). In addition, the transverse nature of the axial diquark propagator is omitted. In spite of this fact, the trend for the baryon octet coincides with our results, also in the larger mass of the Λ with respect to the proton. The decuplet sector is also similar to ours.

In the decuplet sector we find a hierarchy based on the strangeness content, i.e., the T_c increases with the number of constituent strange quarks of the baryon. In this respect the first baryon that melts is the Δ , whereas the Ω has the largest Mott temperature.

The main conclusion of this work is the evident flavor dependence of the deconfinement temperature of baryons. On the qualitative level, our result is quite robust because of the fact that the relative temperatures remain similar for both NJL and PNJL models. On the quantitative side, the Mott temperatures are strongly dependent on the model (NJL or PNJL) used, and in both cases they seem to overestimate the standard values for the freeze-out temperatures obtained by the thermal fits.

Statistical models applied to ALICE data predict a lower chemical freeze-out temperature for proton in comparison with the that for states with multistrangeness (Ξ and Ω). Within our approximation, our findings agree with this claim being the proton temperature 38 MeV (33 MeV) less than the Ξ temperature in the NJL (PNJL) model. This fits well to the experimental findings in [4].

In addition, we find that the temperature of the Ξ and Ω baryons are surprisingly similar, in accordance with the thermal-statistical model result [4]. In our scheme, this result is totally nontrivial, because of the fact that the internal baryon structure is entirely different for the two states, because we have different kinds of constituent diquarks.

In summary, we have applied the NJL and PNJL models, together with different many-body techniques—Bethe-Salpeter and Fadeev equations—to generate diquarks and baryons, respectively. The parameters of the models are fitted to agree with the low-lying states in the respective channel (G_{DIQ} fitted to reproduce the proton mass and $G_{\text{DIQ},V}$ to the Δ baryon mass), being the mass of other baryon predictions of the models.

Extending the method to finite temperature we were able to predict the temperature dependence of baryon masses for all the physical states belonging to the flavor octet and

decuplet representations. We find a strong dependence on the melting (or deconfinement) temperature depending on the flavor content of the baryons. In a qualitative way, our findings coincide with the suggested results on the statistical thermal model on ALICE data [4], and supported by lattice-QCD results by [9].

ACKNOWLEDGMENTS

We acknowledge M. Buballa and L. Tolós for interesting and very useful discussions. This research was supported by the Program TOGETHER from Région Pays de la Loire and the European I3-Hadron Physics program. J.M.T.-R. was also funded by Ministerio de Ciencia e Innovación (Spain) under Contracts No. FPA2010-16963 and No. FPA2013-43425-P.

APPENDIX A: FIERZ TRANSFORMATION

The Fierz transformation allows us to convert the original NJL Lagrangian in Eq. (1)—based on the color-current interaction—into a Lagrangian where the fermion fields are reordered to account for interactions in different color, flavor, and spin sectors.

Even if the Fierz transformation is a well-known tool [32], some differences in its application can be found in the context of the NJL model. The Fierz transformation itself is based on algebraic identities in flavor, color, and spin spaces. It is therefore unique once N_f and N_c are fixed. However, there are at least two methods to obtain the transformed Lagrangian.

The first method requires two different Fierz transformations [11] to obtain all the mesonic and diquark contributions. A Fierz transformation transforms the original color-current interaction to the “exchange sector” containing the $\bar{q}q$ interaction in both color singlet and color octet representations. In color space the transformation reads

$$\sum_{a'=1}^{N_c^2-1} T_{i'j'}^{a'} T_{k'l'}^{a'} = 2 \frac{N_c^2-1}{N_c^2} \delta_{i'l'} \delta_{k'j'} - \frac{1}{N_c} \sum_{a'=1}^{N_c^2-1} T_{i'l'}^{a'} T_{k'j'}^{a'}. \quad (\text{A1})$$

To study physical mesons, one considers the first term, while the second term is simply neglected. A second Fierz transformation is applied to the color-current interaction to

generate the qq sector in both color antitriplet and sextet representations:

$$\sum_{a'=1}^{N_c^2-1} T_{i'j'}^{a'} T_{k'l'}^{a'} = \frac{N_c-1}{N_c} \sum_{S'} T_{i'k'}^{S'} T_{l'j'}^{S'} - \frac{N_c+1}{N_c} \sum_{A'} T_{i'k'}^{A'} T_{l'j'}^{A'}, \quad (\text{A2})$$

where S' and A' run over the symmetric and antisymmetric members of the color representation, respectively. For $N_c = 3$, $S' = 1, 3, 4, 6, 8$, and $A' = 2, 5, 7$. The first term is neglected as it contains a repulsive diquark interaction and is not useful to generate colorless baryons.

The second method makes use of only one Fierz transformation [14,33] which follows from the principle of obtaining only attractive-color interactions. With this prescription, the final Lagrangian for both mesons and diquarks is obtained by a single Fierz transformation in color space:

$$\sum_{a'=1}^{N_c^2-1} T_{i'j'}^{a'} T_{k'l'}^{a'} = \frac{N_c-1}{2N_c} \delta_{i'l'} \delta_{j'k'} - \frac{2}{N_c} \sum_{A'} T_{i'k'}^{A'} T_{l'j'}^{A'}. \quad (\text{A3})$$

In the right-hand side of Eq. (A3), the first term produces the Lagrangian for mesons in the color singlet representation, and the second one the Lagrangian for diquarks in the color antitriplet-color representation. No sign of any $\bar{q}q$ interaction in the color octet and of the qq one in the color sextet is seen. As claimed, these channels are not needed to obtain physical mesons and the baryonic states.

Notice that the numerical factors appearing in front of the Fierz Lagrangian depend on the choice of the method. Therefore, they present different values for the coupling constants. However, we remind the reader that we are treating these couplings as free parameters to be fixed by reproducing the hadron masses. For this reason the two methods are equivalent, if the coupling constant is considered as a free parameter.

In this work we will use the conventions given in Ref. [11] and generate all possible interactions in the qq and in the $\bar{q}q$ sectors. The terms which we obtain are in exact correspondence with the irreducible representations of the flavor and color group products.

For the meson sector the Fierz-transformed Lagrangian reads [11] (we suppress the flavor indices i, j)

$$\begin{aligned} \mathcal{L}_{ex} = & \frac{2(N_c^2-1)}{N_f N_c^2} g [(\bar{\psi}\psi)^2 + (\bar{\psi}i\gamma_5\psi)^2 - \frac{1}{2}(\bar{\psi}\gamma^\mu\psi)^2 - \frac{1}{2}(\bar{\psi}\gamma^\mu\gamma_5\psi)^2] \\ & + \frac{N_c^2-1}{N_c^2} \mathbf{g} [(\bar{\psi}\tau^a\psi)^2 + (\bar{\psi}i\gamma_5\tau^a\psi)^2 - \frac{1}{2}(\bar{\psi}\gamma^\mu\tau^a\psi)^2 - \frac{1}{2}(\bar{\psi}\gamma^\mu\gamma_5\tau^a\psi)^2] \\ & - \frac{1}{N_f N_c} g [(\bar{\psi}T^{a'}\psi)^2 + (\bar{\psi}i\gamma_5 T^{a'}\psi)^2 - \frac{1}{2}(\bar{\psi}\gamma^\mu T^{a'}\psi)^2 - \frac{1}{2}(\bar{\psi}\gamma^\mu\gamma_5 T^{a'}\psi)^2] \\ & - \frac{1}{2N_c} g [(\bar{\psi}\tau^a T^{a'}\psi)^2 + (\bar{\psi}i\gamma_5\tau^a T^{a'}\psi)^2 - \frac{1}{2}(\bar{\psi}\gamma^\mu\tau^a T^{a'}\psi)^2 - \frac{1}{2}(\bar{\psi}\gamma^\mu\gamma_5\tau^a T^{a'}\psi)^2], \end{aligned} \quad (\text{A4})$$

where $a = 1, \dots, N_f^2 - 1$ and $a' = 1, \dots, N_c^2 - 1$. It is not difficult to check that the different terms match with the representations spanned by

$$(\mathbf{3} \otimes \bar{\mathbf{3}})_c \otimes (\mathbf{3} \otimes \bar{\mathbf{3}})_f \otimes \{1, i\gamma_5, \gamma_\mu, \gamma_5\gamma_\mu\}. \quad (\text{A5})$$

The second row (in bold font) will be of interest to produce the physical mesons. In particular, the second term is the relevant one for the pseudoscalar mesons (π, K , and η).

Performing the second Fierz transformation one obtains the diquark sector [11]:

$$\begin{aligned} \mathcal{L}_{qq} = & \frac{N_c + 1}{2N_c} g \left[(\bar{\psi} \mathbf{i} \gamma_5 \mathbf{C} \tau^A \mathbf{T}^{A'} \bar{\psi}^T) (\psi^T \mathbf{C} \mathbf{i} \gamma_5 \tau^A \mathbf{T}^{A'} \psi) + (\bar{\psi} \mathbf{C} \tau^A T^{A'} \bar{\psi}^T) (\psi^T \mathbf{C} \tau^A T^{A'} \psi) \right. \\ & \left. - \frac{1}{2} (\bar{\psi} \gamma^\mu \gamma_5 \mathbf{C} \tau^A T^{A'} \bar{\psi}^T) (\psi^T \mathbf{C} \gamma_\mu \gamma_5 \tau^A T^{A'} \psi) - \frac{1}{2} (\bar{\psi} \gamma^\mu \mathbf{C} \tau^S \mathbf{T}^{A'} \bar{\psi}^T) (\psi^T \mathbf{C} \gamma_\mu \tau^S \mathbf{T}^{A'} \psi) \right] \\ & - \frac{N_c - 1}{2N_c} g \left[(\bar{\psi} \mathbf{i} \gamma_5 \mathbf{C} \tau^S T^{S'} \bar{\psi}^T) (\psi^T \mathbf{C} \mathbf{i} \gamma_5 \tau^S T^{S'} \psi) + (\bar{\psi} \mathbf{C} \tau^S T^{S'} \bar{\psi}^T) (\psi^T \mathbf{C} \tau^S T^{S'} \psi) \right. \\ & \left. - \frac{1}{2} (\bar{\psi} \gamma^\mu \gamma_5 \mathbf{C} \tau^S T^{S'} \bar{\psi}^T) (\psi^T \mathbf{C} \gamma_\mu \gamma_5 \tau^S T^{S'} \psi) - \frac{1}{2} (\bar{\psi} \gamma^\mu \mathbf{C} \tau^A T^{S'} \bar{\psi}^T) (\psi^T \mathbf{C} \gamma_\mu \tau^A T^{S'} \psi) \right], \end{aligned} \quad (\text{A6})$$

where the indices A, A' refer to the antisymmetric members of the flavor and color representations, respectively, and the indices S, S' to the symmetric elements of the flavor and color representations. In this way, the Fierz transformation in the qq sector generates the eight possible terms consistent with the direct product of

$$\mathcal{A}[(\mathbf{3} \otimes \mathbf{3})_c \otimes (\mathbf{3} \otimes \mathbf{3})_f \otimes \{1, i\gamma_5, \gamma_\mu, \gamma_5 \gamma_\mu\}], \quad (\text{A7})$$

where \mathcal{A} denotes the antisymmetrization operator to respect the Pauli principle for the exchange of two quarks. In Eq. (A6) we highlight the two terms giving rise to the scalar and axial diquark discussed in this work when forming baryons.

APPENDIX B: QUARK CONDENSATE AND MESON POLARIZATION FUNCTION

For completeness, we include here some reduced expressions for the quark condensate in Eq. (8) and the meson polarization function in Eq. (38). For practical reasons we remind the reader of the A and B_0 functions introduced in Refs. [22,34]. These functions are convenient for implementing numerically the momentum integrations for the thermal averages.

For vanishing chemical potentials, the function A is defined as

$$A(m_i, T, \Lambda) \equiv 16\pi^2 T \sum_n \int \frac{d^3k}{(2\pi)^3} \frac{1}{(i\omega_n)^2 - E_i^2}, \quad (\text{B1})$$

with the quark energy $E_i = \sqrt{k^2 + m_i^2}$ and the fermionic Matsubara frequencies $i\omega_n = i(2n+1)\pi T$. This function naturally appears when computing the quark condensate defined in Eq. (8):

$$\langle \bar{\psi}_i \psi_i \rangle = N_c \frac{m_i}{4\pi^2} A(m_i, T, \Lambda). \quad (\text{B2})$$

Performing the Matsubara summation [35] one obtains

$$\begin{aligned} A(m_i, T, \Lambda) &= -16\pi^2 \int \frac{d^3k}{(2\pi)^3} \frac{1}{2E_i} [1 - 2n_F(E_i)] \\ &= 4 \int_{m_i}^{\Lambda_E} dE_i \sqrt{E_i^2 - m_i^2} [n_F(E_i) - n_F(-E_i)], \end{aligned} \quad (\text{B3})$$

where $n_F(E_i) = (e^{E_i/T} + 1)^{-1}$ is the Fermi-Dirac distribution function and $\Lambda_E = \sqrt{\Lambda^2 + m_i^2}$. For the PNJL model one simply replaces Eq. (B2) by Eq. (20).

The function B_0 is defined as

$$\begin{aligned} B_0(m_i, m_j, i\nu_m, \mathbf{p}, T, \Lambda) \\ = 16\pi^2 T \sum_n \int \frac{d^3k}{(2\pi)^3} \frac{1}{(i\omega_n)^2 - E_i^2} \frac{1}{(i\omega_n - i\nu_m) - E_j^2}, \end{aligned} \quad (\text{B4})$$

with $E_i = \sqrt{k^2 + m_i^2}$ and $E_j = \sqrt{(\mathbf{k} - \mathbf{p})^2 + m_j^2}$. It naturally appears in the quark-(anti)quark loop function, when computing the diquark (meson) polarization function. After performing the Matsubara summation, the Matsubara frequency $i\nu_m$ is analytically continued to real values of the energy with the prescription $i\nu_m \rightarrow p_0 + i\epsilon$. For instance, the pion polarization function ($m_i = m_u, m_j = m_d$) can be expressed as a combination of the A and B_0 functions as

$$\begin{aligned} \Pi^{ud}(p_0, \mathbf{p}, m_u, m_d, T, \Lambda) \\ = -\frac{N_c}{4\pi^2} \{A(m_u, T, \Lambda) + A(m_d, T, \Lambda) \\ + [(m_u - m_d)^2 - p_0^2 + \mathbf{p}^2] B_0(m_u, m_d, p_0, \mathbf{p}, T, \Lambda)\}. \end{aligned} \quad (\text{B5})$$

In the case of a pion at rest, $\mathbf{p} = 0$, one can perform the Matsubara summation and finds

$$\begin{aligned} B_0(m_i, m_j, p_0, 0, T, \Lambda) = \sum_{\sigma=\pm} \sigma [B_0^\sigma(m_i, m_j, -\sigma p_0, T, \Lambda) \\ + B_0^\sigma(m_j, m_i, \sigma p_0, T, \Lambda)], \end{aligned} \quad (\text{B6})$$

where

$$\Re B_0^\pm(m_i, m_j, p_0, T, \Lambda) = \frac{2}{p_0} \text{P.V.} \int_{m_i}^{\Lambda_E} dE_i \sqrt{E_i^2 - m_i^2} \frac{n_F(\pm E_i)}{E_i - E_0}, \quad (\text{B7})$$

$$\Im B_0^\pm(m_i, m_j, p_0, T, \Lambda) = \frac{2\pi}{p_0} \sqrt{E_0^2 - m_i^2} n_F(\pm E_0) \Theta(\Lambda_E - E_0) \Theta(E_0 - m_i), \quad (\text{B8})$$

$$\text{with } E_0 \equiv -(p_0^2 + m_i^2 - m_j^2)/(2p_0).$$

Let us briefly discuss some of the prescriptions to define the mass and decay width of the mesons and diquarks.

These generated states are identified with the poles of the scattering amplitude $t^{ab}(p^2)$, or Eq. (42). We can distinguish those states that are generated below and above the two-quark mass threshold, that is, those which cannot decay into a pair of quarks and those in which this decay channel is open because their mass is larger than the combined mass of the constituents.

In the first case we talk of “bound states” (the decay width is exactly zero). For them, the polarization function is a real function (B_0 does not develop any imaginary part) and the pole is generated on the real axis of the p_0 plane (in the first Riemann sheet). The real value of p_0 is associated with the mass of the bound state. In the second case we denote them as “resonances” (a finite decay width is generated), the polarization function is now complex [Eq. (B8) is nonzero] and the pole emerges at a complex p_0 (in the second Riemann sheet). The imaginary part of the pole can be related to the decay width of the resonance.

At finite temperature, the variable $p_0 = i\nu_m$ is strictly a Matsubara frequency. If a bound state is generated, then one can simply make the standard analytical continuation to real energies $i\nu_m \rightarrow p_0 + i\epsilon$ and find the value of the generated mass by solving $1 - 2K^{ab}\Pi^{ab}(p_0) = 0$, with real $\Pi^{ab}(p_0)$. However, for a resonant state, one must analytically continue the Matsubara frequency to complex energies and find the pole in the second Riemann sheet. As this procedure might be cumbersome (in particular for cases with several coupled channels, where additional Riemann sheets must be considered), approximate methods are used (see, for instance, [19]).

One introduces the spectral density $\rho(p_0, \mathbf{p})$ (see [36], for instance) as the imaginary part of the bound state/resonance propagator,

$$\begin{aligned} \rho^{ab}(p_0, \mathbf{p}) &= -\frac{1}{\pi} \text{Im} t^{ab}(p_0, \mathbf{p}) \\ &= \frac{1}{\pi} \frac{\text{Im} \Pi^{ab}(p_0, \mathbf{p})}{[(2G)^{-1} - \Pi^{ab}(p_0, \mathbf{p})]^2 + [\text{Im} \Pi^{ab}(p_0, \mathbf{p})]^2}, \end{aligned} \quad (\text{B9})$$

where the Matsubara frequencies have been analytically continued to real energies. Therefore, the spectral function is a real function of real argument.

Note that taking $\mathbf{p} = 0$, using the pole approximation and the optical theorem we can check that the spectral function is proportional to the scattering amplitude squared evaluated on the real axis,

$$\rho^{ab}(p_0, 0) = -\frac{1}{\pi} \text{Im} t^{ab}(p_0, 0) \propto |T|^2(p_0, 0). \quad (\text{B10})$$

Thus, whenever the scattering amplitude presents a pole, this is reflected into the spectral function as a peak. If the pole is not far from the real axis ($\text{Im} p_0 \ll \text{Re} p_0$), the real part of p_0 at the pole position coincides with the maximum of the spectral function. Therefore, the mass can be defined as the position of the spectral density maximum. If, in addition, $\text{Im} \Pi^{ab}(p_0)$ is a smooth function of p_0 [36] around the peak, it can be approximated by a Lorentzian shape, with a width [19,36],

$$\Gamma = -\text{Im} \Pi^{ab}(p_0). \quad (\text{B11})$$

In this approximation, one defines the decay width of the resonance as the Lorentzian width Γ .

However, this approximation might break down if the pole position is far away from the real axis, and in particular, if the many-body equation presents coupled channels: a broad resonance can be hidden by another pole with more strength in this channel, several poles might appear very close in the complex plane producing a combined shape of the the spectral function, a new threshold opens close to the resonance (Flatté effect) blurring the Lorentzian shape, etc.

As in this paper we are not interested in a precise extraction of the decay widths but only in the temperature at which they become nonzero, we use an intermediate prescription described in Ref. [22,34]. In this case one makes the analytical continuation to real energies (after having performed the Matsubara summation) but considers a complex p_0 in the factor in front of the B_0 function in Eq. (B5). This prescription provides a complex polarization function of complex argument and one has direct access to the mass ($m = \text{Re} p_0$) and decay width ($\Gamma = -2\text{Im} p_0$) of the resonant state.

APPENDIX C: BETHE-SALPETER EQUATION FOR QUARK-QUARK SCATTERING

The Bethe-Salpeter equation for the qq scattering [12,23,37] in the scalar channel reads Eq. (46)

$$\begin{aligned} T_{ij,mn}^{ab}(p^2) &= \mathcal{K}_{ij,mn}^{ab} + i \int \frac{d^4 k}{(2\pi)^4} \mathcal{K}_{ij,pq}^{ac} S_p \left(k + \frac{p}{2} \right) \\ &\quad \times S_q \left(\frac{p}{2} - k \right) T_{pq,mn}^{cb}(p^2). \end{aligned} \quad (\text{C1})$$

We can pull out all the vertex factors by defining the diquark propagator t_{ab} ,

$$T_{ij,mn}^{ab}(p^2) = \Omega_{ij}^a t^{ab}(p^2) \bar{\Omega}_{nm}^b, \quad (\text{C2})$$

where

$$\Omega_{ij}^a = T^{a'} \otimes \tau_{ij}^a \otimes \Gamma C, \quad (\text{C3})$$

with $\Gamma = i\gamma_5\gamma_\mu$ for scalar and axial diquarks, respectively, $C = i\gamma_0\gamma_2$ being the charge conjugation operator.

The kernel is taken from the Fierz NJL Lagrangian of Eq. (44),

$$\mathcal{K}_{ij,mn}^{ab} = \Omega_{ij}^a 2G_{DIQ} \bar{\Omega}_{nm}^b, \quad (\text{C4})$$

where the 2 is a combinatorial factor arising when attaching the external legs to the vertex and G_{DIQ} must be substituted by $G_{DIQ,V}$ for axial diquarks. Note that we neglect any contribution from the 't Hooft Lagrangian as there is no flavor singlet in this channel and its effects are expected to be much suppressed (there is a small effect around 4 %, discussed in Ref. [12]).

In terms of the amplitude $t(p^2)$ we can express the solution of the BS equation for scalar diquarks,

$$t^{ab}(p^2) = \frac{2G_{DIQ}}{1 - 2G_{DIQ}\Pi^{ab}(p^2)}, \quad (\text{C5})$$

with the polarization function,

$$\Pi^{ab}(p^2) = i \int \frac{d^4k}{(2\pi)^4} \text{Tr} [\bar{\Omega}_{ji}^a S_i(k + p/2) \Omega_{ij}^b S_j^T(p/2 - k)], \quad (\text{C6})$$

where the trace is to be taken in color, flavor, and Dirac spaces. For axial diquarks, the amplitude involves the transverse part of the polarization function [cf. Eq. (49)],

$$t^{ab}(p^2) = \frac{2G_{\text{DIQ},V}}{1 - 2G_{\text{DIQ},V}\Pi_{\perp}^{ab}(p^2)}. \quad (\text{C7})$$

For the scalar case one has

$$\begin{aligned} \Pi^{ab}(p^2) = & \text{tr}_c(T^{a'} T^{b'}) \tau_{ji}^a \tau_{ij}^b i \int \frac{d^4k}{(2\pi)^4} \text{tr}_\gamma \\ & \times \left[i\gamma_5 S_i \left(k + \frac{p}{2} \right) i\gamma_5 C S_j^T \left(\frac{p}{2} - k \right) C^{-1} \right]. \end{aligned} \quad (\text{C8})$$

The color factor is common to all diquarks in the antitriplet color representation, where the generators can be taken as [12]

$$(T^{a'})_{j'k'} = i\epsilon_{a'j'k'}. \quad (\text{C9})$$

The color factor reads

$$\text{tr}_c(T^{a'} T^{b'}) = - \sum_{k'l'} \epsilon^{a'k'l'} \epsilon^{b'l'k'} = 2\delta^{a'b'}, \quad (\text{C10})$$

which means that the color of the diquark does not change in the propagation. From now on we will suppress the color indices.

Using the identity,

$$C S_i^T \left(\frac{p}{2} - k \right) C^{-1} = S_i \left(k - \frac{p}{2} \right), \quad (\text{C11})$$

we can express the polarization function as

$$\Pi^{ab}(p^2) = 2 \tau_{ji}^a \tau_{ij}^b i \int \frac{d^4k}{(2\pi)^4} \text{tr}_\gamma [i\gamma_5 S_i(k) i\gamma_5 S_j(k - p)], \quad (\text{C12})$$

where we have performed a variable shift $k \rightarrow k - p/2$.

In flavor space, we choose the representations shown in Table VI for the sextet and antitriplet case [12,38]. For both of them, the normalization is $\text{tr}(\tau^a \tau^b) = 2\delta^{ab}$.

As an example, we calculate the lightest $a = [ud]$ diquark. It is easy to see that the polarization function is diagonal in flavor, so the only possibility is to have $b = [ud]$. Using $\tau_{ij}^{[ud]} = -\lambda_{ij}^2$,

$$\Pi^{[ud]}(p^2) = 4i \int \frac{d^4k}{(2\pi)^4} \text{tr}_\gamma [i\gamma_5 S_d(k) i\gamma_5 S_u(k - p)]. \quad (\text{C13})$$

This is the final expression for the polarization function that gives rise to the propagator of the $[ud]$ diquark.

At finite temperature, we introduce fermionic Matsubara frequencies,

$$\begin{aligned} \Pi^{[ud]}(i\nu_m, \mathbf{p}) = & -4T \sum_n \int \frac{d^3k}{(2\pi)^3} \text{tr}_\gamma \\ & \times [i\gamma_5 S_d(i\omega_n, \mathbf{k}) i\gamma_5 S_u(i\omega_n - i\nu_m, \mathbf{k} - \mathbf{p})]. \end{aligned} \quad (\text{C14})$$

TABLE VI. Flavor matrices for the antitriplet and sextet flavor representations of the direct product $\mathbf{3}_f \otimes \mathbf{3}_f$ of $SU(3)$.

Physical diquark	$\bar{\mathbf{3}}$ Representation
$[ud]$	$\tau_{ij}^{[ud]} = \tau_{ij}^{\bar{\mathbf{3}}} = -\lambda_{ij}^2$
$[us]$	$\tau_{ij}^{[us]} = \tau_{ij}^{\bar{\mathbf{3}}} = \lambda_{ij}^5$
$[ds]$	$\tau_{ij}^{[ds]} = \tau_{ij}^{\bar{\mathbf{3}}} = -\lambda_{ij}^7$
Physical diquark	$\mathbf{6}$ Representation
(uu)	$\tau_{ij}^{(uu)} = \tau_{ij}^{\mathbf{6}} = \sqrt{2}\delta_{i1}\delta_{j1}$
(ud)	$\tau_{ij}^{(ud)} = \tau_{ij}^{\mathbf{6}} = \lambda_{ij}^1$
(dd)	$\tau_{ij}^{(dd)} = \tau_{ij}^{\mathbf{6}} = \sqrt{2}\delta_{i2}\delta_{j2}$
(us)	$\tau_{ij}^{(us)} = \tau_{ij}^{\mathbf{6}} = \lambda_{ij}^4$
(ds)	$\tau_{ij}^{(ds)} = \tau_{ij}^{\mathbf{6}} = \lambda_{ij}^6$
(ss)	$\tau_{ij}^{(ss)} = \tau_{ij}^{\mathbf{6}} = \sqrt{2}\delta_{i3}\delta_{j3}$

After performing the Matsubara sum, we analytically continue the unsummed Matsubara frequency $i\nu_m$ to the real energy $p_0 + i\epsilon$. For practical purposes, this function can be reduced in terms of the A, B_0 functions defined in [22,34] and detailed in Appendix B:

$$\begin{aligned} \Pi^{[ud]}(p_0, \mathbf{p}) = & -\frac{1}{2\pi^2} \{A(m_u, T, \Lambda) + A(m_d, T, \Lambda) + [(m_u - m_d)^2 \\ & - p_0^2 + \mathbf{p}^2] B_0(m_u, m_d, p_0, \mathbf{p}, T, \Lambda)\}. \end{aligned}$$

Similar expressions can be found for other diquarks in different flavor channels.

For axial diquarks, the expression for the transverse part of the polarization function reads

$$\begin{aligned} \Pi_{\perp}^{(ud)}(p_0, \mathbf{p}) = & \frac{1}{3\pi^2} \{A(m_u, T, \Lambda) + A(m_d, T, \Lambda) + [(m_u - m_d)^2 \\ & - 2m_u m_d - p_0^2 + \mathbf{p}^2] B_0(m_u, m_d, p_0, \mathbf{p}, T, \Lambda)\}. \end{aligned}$$

APPENDIX D: REDUCTION OF THE FADEEV EQUATION

In this appendix we will give some details of the simplification of the Fadeev equation in Eq. (57) and its reduction to a Dirac equation. We follow the same reasoning as in Ref. [13], but with a different notation.

We start by considering Eq. (57):

$$\begin{aligned} & \left[g^{\alpha\beta} \delta_{j'k'} \delta^{\bar{j}k'} \delta_{jk} \delta^{\bar{j}k} - \int \frac{d^4k}{(2\pi)^4} L_{jk}^{\bar{j}k, \alpha\beta}(P^2, q, k) \right] \\ & \times X_k^{\bar{k}\beta}(P^2, q) \Big|_{P^2=M_B^2} = 0, \end{aligned} \quad (\text{D1})$$

where its kernel was defined in Eq. (58). Notice that we have denoted the color terms of the equation by primed indices, to distinguish them from flavor factors.

For convenience, we define a new baryon wave function Y by integrating over the momentum q [13],

$$Y_k^{\bar{k}\beta}(P^2) \equiv \int \frac{d^4q}{(2\pi)^4} X_k^{\bar{k}\beta}(P^2, q). \quad (\text{D2})$$

To express the Fadeev equation in terms of the new wave function one integrates Eq. (D1) over q to get

$$\left[g^{\alpha\beta} \delta_{j'k'} \delta^{j'\bar{k}'} \delta_{jk} \delta^{j\bar{k}} Y_k^{\bar{k}\beta}(P^2) - \int \frac{d^4q}{(2\pi)^4} \right. \\ \times \int \frac{d^4k}{(2\pi)^4} T_{j'l'}^{\bar{k}'} \tau_{jl}^{\bar{k}} \Gamma^\nu S_l(-q-k) T_{l'k}^{\bar{j}} \tau_{lk}^{\bar{j}} \\ \left. \times \Gamma^\alpha S_k(P/2+q) i t_k^{\nu\beta}(P/2-q) X_k^{\bar{k}\beta}(P^2, k) \right] \Big|_{P^2=m_B^2} = 0,$$

where we have substituted the kernel given in Eq. (58). Notice that it is not possible to express the equation only in terms of $Y_k^{\bar{k}\beta}(P^2)$ because there is a quark propagator that depends on the momentum k . Therefore, this equation is nonseparable and can be only solved with numerical techniques [28].

In the so-called ‘‘static approximation’’ [13] one neglects the momentum dependence of the quark propagator by assuming that the dress quark mass is much larger than the typical k :

$$S_l(-q-k) = \frac{1}{-q - \not{k} - m_l} \rightarrow \frac{-1}{m_l} \mathbb{I}. \quad (\text{D3})$$

This approximation makes the Fadeev equation separable, and allows for a trivial integration on k . The equation is reduced to the simpler form:

$$\left[g^{\alpha\beta} \delta_{j'k'} \delta^{j'\bar{k}'} \delta_{jk} \delta^{j\bar{k}} + \int \frac{d^4q}{(2\pi)^4} T_{j'l'}^{\bar{k}'} T_{l'k}^{\bar{j}} \tau_{jl}^{\bar{k}} \tau_{lk}^{\bar{j}} \Gamma^\mu \Gamma_\mu \frac{1}{m_l} \right. \\ \left. \times S_k\left(\frac{P}{2}+q\right) i t_k^{\alpha\beta}\left(\frac{P}{2}-q\right) \right] Y_k^{\bar{k}\beta}(P^2) \Big|_{P^2=m_B^2} = 0.$$

To obtain the baryon masses of the different states, we project this equation onto physical states B and B' . The flavor projectors are defined in Appendix E for those states belonging to the octet and the decuplet representations. Applying these projectors we find

$$\delta_{jk} \delta^{j\bar{k}} \mathcal{P}_{j\bar{j}}^{B,\dagger} \mathcal{P}_{\bar{k}k}^{B'} = \mathcal{P}_{j\bar{j}}^{B,\dagger} \mathcal{P}_{\bar{k}k}^{B'} = \delta^{BB'}. \quad (\text{D4})$$

In color space we take the projector onto the singlet state, $\mathcal{P}_{j\bar{j}}^{\text{color}} = \delta_{j\bar{j}}/\sqrt{3}$. In the first term of Eq. (4) one has

$$\mathcal{P}_{j\bar{j}}^{\text{color},\dagger} \delta_{j'k'} \delta^{j'\bar{k}'} \mathcal{P}_{\bar{k}k}^{\text{color},\dagger} = \frac{1}{3} \text{tr}_c \mathbb{I} = 1, \quad (\text{D5})$$

whereas in the second term of Eq. (4),

$$\mathcal{P}_{j\bar{j}}^{\text{color},\dagger} T_{j'l'}^{\bar{k}'} T_{l'k}^{\bar{j}} \mathcal{P}_{\bar{k}k}^{\text{color},\dagger} = \frac{1}{3} T_{j'l'}^{\bar{k}'} T_{l'k}^{\bar{j}} = -2, \quad (\text{D6})$$

where we have used Eq. (C9).

To simplify the notation we can define the matrix $M^{BB'}$,

$$M^{BB',\alpha\beta}(P) \equiv \frac{2}{m_l} \int \frac{d^4q}{(2\pi)^4} \mathcal{P}_{j\bar{j}}^{\dagger,B} \mathcal{P}_{\bar{k}k}^{B'} \tau_{jl}^{\bar{k}} \tau_{lk}^{\bar{j}} \Gamma^\mu \Gamma_\mu \\ \times S_k\left(\frac{P}{2}+q\right) i t_k^{\alpha\beta}\left(\frac{P}{2}-q\right). \quad (\text{D7})$$

The final equation is expressed as a Dirac-like equation,

$$g^{\alpha\beta} \delta^{BB'} - M^{BB',\alpha\beta}(P^2 = M_B^2) = 0, \quad (\text{D8})$$

which is a matrix equation in Dirac and flavor spaces.

For the baryon octet (composed by scalar diquarks) the α, β -Lorentz indices are absent and $\Gamma^\mu = i\gamma^5$. Therefore one has (after performing the change of variables $q \rightarrow -q + P/2$)

$$M^{BB'}(P) = -\frac{2}{m_l} \mathcal{P}_{j\bar{j}}^{\dagger,B} \mathcal{P}_{\bar{k}k}^{B'} \tau_{jl}^{\bar{k}} \tau_{lk}^{\bar{j}} \int \frac{d^4q}{(2\pi)^4} S_k(P-q) i t_{\bar{k}}(q), \quad (\text{D9})$$

where the scalar diquark propagator $t_{\bar{k}}$ is taken from Eq. (52).

In flavor space this equation is diagonal except for the $\Lambda - \Sigma^0 - \mathbb{I}$ mixing, where one needs to solve

$$\det \begin{pmatrix} 1 - M^{\Sigma^0 \Sigma^0} & -M^{\Sigma^0 \Lambda} & -M^{\Sigma^0 \mathbb{I}} \\ -M^{\Lambda \Sigma^0} & 1 - M^{\Lambda \Lambda} & -M^{\Lambda \mathbb{I}} \\ -M^{\mathbb{I} \Sigma^0} & -M^{\mathbb{I} \Lambda} & 1 - M^{\mathbb{I} \mathbb{I}} \end{pmatrix} = 0. \quad (\text{D10})$$

In the isospin limit ($m_u = m_d$) one has $M^{\mathbb{I} \Sigma^0} = M^{\Sigma^0 \mathbb{I}} = M^{\Lambda \Sigma^0} = M^{\Sigma^0 \Lambda} = 0$. Thus, the Σ^0 decouples from the system (D10), and in this limit its mass is degenerate with the mass of the Σ^+ baryon. However, the elements $M^{\mathbb{I} \Lambda}$ and $M^{\Lambda \mathbb{I}}$ are nonzero and this produces a mixing between the flavor singlet and the Λ . Therefore, to obtain the mass of the Λ we need to solve the two-channel equation.

For the members of the decuplet (composed by axial diquarks) one uses $\Gamma^\mu = \gamma^\mu$ to get

$$M^{BB',\alpha\beta}(P) \equiv \frac{8}{m_l} \mathcal{P}_{j\bar{j}}^{\dagger,B} \mathcal{P}_{\bar{k}k}^{B'} \tau_{jl}^{\bar{k}} \tau_{lk}^{\bar{j}} \int \frac{d^4q}{(2\pi)^4} S_k(P-q) i t_{\bar{k}}^{\alpha\beta}(q), \quad (\text{D11})$$

with the diquark propagator taken from Eq. (54). In this case, the Eq. (D8) is diagonal in flavor space.

APPENDIX E: PHYSICAL BARYON PROJECTIONS

Baryon masses are computed by solving the Fadeev equation projected into the different physical states. The baryon projectors project the general wave function onto the wave functions of specific baryons. In our scheme, the baryon wave functions are the direct product of quark and diquarks wave functions. In this appendix we provide the precise expressions for completeness [39,40].

In Table VII we present the baryon octet and decuplet wave functions in terms of the quark-diquark states. As in the main text, scalar diquarks are represented by square brackets and axial diquarks by parentheses. We remind one that in this work we neglect the axial-diquark contribution to the members of baryon octet.

These wave functions help us to construct the baryon projectors. They satisfy

$$(\mathcal{P}_{ij}^B)^\dagger = \mathcal{P}_{ji}^B, \quad (\text{E1})$$

where B represents the physical baryon state. They are orthonormal within the same representation,

$$(\mathcal{P}_{ji}^B)^\dagger \mathcal{P}_{ij}^{B'} = \delta^{BB'}. \quad (\text{E2})$$

For the baryon octet they read

$$\mathcal{P}_{ij}^p = \frac{1}{2} (\lambda^4 - i\lambda^5)_{ij}, \quad (\text{E3})$$

TABLE VII. Baryon wave functions for all the members of the octet and decuplet flavor representations.

Octet member	Wave function	Decuplet member	Wave function
p	$ u[ud]\rangle$	Δ^{++}	$ u(uu)\rangle$
n	$ d[ud]\rangle$	Δ^+	$\frac{1}{\sqrt{3}}(d(uu)\rangle + \sqrt{2} u(ud)\rangle)$
Λ	$\frac{1}{\sqrt{6}}(u[ds]\rangle + d[us]\rangle - 2 s[ud]\rangle)$	Δ^0	$\frac{1}{\sqrt{3}}(\sqrt{2} d(ud)\rangle + u(dd)\rangle)$
Σ^+	$ u[us]\rangle$	Δ^-	$ d(dd)\rangle$
Σ^0	$\frac{1}{\sqrt{2}}(u[ds]\rangle - d[us]\rangle)$	Σ^*	$\frac{1}{\sqrt{3}}(s(uu)\rangle + \sqrt{2} u(us)\rangle)$
Σ^-	$ d[ds]\rangle$	Σ^{*0}	$\frac{1}{\sqrt{3}}(s(ud)\rangle + d(us)\rangle + u(ds)\rangle)$
Ξ^0	$ s[us]\rangle$	Σ^{*-}	$\frac{1}{\sqrt{3}}(s(dd)\rangle + \sqrt{2} d(ds)\rangle)$
Ξ^-	$ s[ds]\rangle$	Ξ^{*0}	$\frac{1}{\sqrt{3}}(\sqrt{2} s(us)\rangle + u(ss)\rangle)$
Singlet	Wave function	Ξ^{*-}	$\frac{1}{\sqrt{3}}(\sqrt{2} s(ds)\rangle + d(ss)\rangle)$
\mathbb{I}	$\frac{1}{\sqrt{3}}(u[ds]\rangle + d[us]\rangle + s[ud]\rangle)$	Ω^-	$ s(ss)\rangle$

$$\mathcal{P}_{ij}^n = \frac{1}{2}(\lambda^6 - i\lambda^7)_{\bar{i}j}, \quad (\text{E4})$$

$$\mathcal{P}_{ij}^\Lambda = \mathcal{P}_{ij}^8 = \sqrt{\frac{1}{2}}\lambda_{\bar{i}j}^8, \quad (\text{E5})$$

$$\mathcal{P}_{ij}^{\Sigma^0} = \mathcal{P}_{ij}^3 = \sqrt{\frac{1}{2}}\lambda_{\bar{i}j}^3, \quad (\text{E6})$$

$$\mathcal{P}_{ij}^{\Sigma^\pm} = \frac{1}{2}(\lambda^1 \mp i\lambda^2)_{\bar{i}j}, \quad (\text{E7})$$

$$\mathcal{P}_{ij}^{\Xi^0} = \frac{1}{2}(\lambda^6 + i\lambda^7)_{\bar{i}j}, \quad (\text{E8})$$

$$\mathcal{P}_{ij}^{\Xi^-} = \frac{1}{2}(\lambda^4 + i\lambda^5)_{\bar{i}j}. \quad (\text{E9})$$

Finally, we need the projector for the flavor singlet state,

$$\mathcal{P}_{ij}^{\mathbb{I}} = \sqrt{\frac{1}{3}}\mathbb{I}_{\bar{i}j}. \quad (\text{E10})$$

Note that for the baryon octet, the diquark index \bar{i} runs from 1 to 3 because the scalar diquark belongs to the antitriplet representation of $SU_f(3) \times SU_f(3)$. In particular, the $[ds]$, $[us]$, and $[ud]$ diquarks are represented by $\bar{i} = 1, 2, 3$, respectively.

For the baryon decuplet the projectors read

$$\mathcal{P}_{ij}^{\Delta^{++}} = \delta_{\bar{i}1}\delta_{j1}, \quad (\text{E11})$$

$$\mathcal{P}_{ij}^{\Delta^+} = \frac{1}{\sqrt{3}}\delta_{\bar{i}1}\delta_{j2} + \sqrt{\frac{2}{3}}\delta_{\bar{i}2}\delta_{j1}, \quad (\text{E12})$$

$$\mathcal{P}_{ij}^{\Delta^0} = \sqrt{\frac{2}{3}}\delta_{\bar{i}2}\delta_{j2} + \frac{1}{\sqrt{3}}\delta_{\bar{i}3}\delta_{j1}, \quad (\text{E13})$$

$$\mathcal{P}_{ij}^{\Delta^-} = \delta_{\bar{i}3}\delta_{j2}, \quad (\text{E14})$$

$$\mathcal{P}_{ij}^{\Sigma^{*+}} = \frac{1}{\sqrt{3}}\delta_{\bar{i}1}\delta_{j3} + \sqrt{\frac{2}{3}}\delta_{\bar{i}4}\delta_{j1}, \quad (\text{E15})$$

$$\mathcal{P}_{ij}^{\Sigma^{*0}} = \frac{1}{\sqrt{3}}(\delta_{\bar{i}2}\delta_{j3} + \delta_{\bar{i}4}\delta_{j2} + \delta_{\bar{i}5}\delta_{j1}), \quad (\text{E16})$$

$$\mathcal{P}_{ij}^{\Sigma^{*-}} = \frac{1}{\sqrt{3}}\delta_{\bar{i}3}\delta_{j3} + \sqrt{\frac{2}{3}}\delta_{\bar{i}5}\delta_{j2}, \quad (\text{E17})$$

$$\mathcal{P}_{ij}^{\Xi^{*0}} = \sqrt{\frac{2}{3}}\delta_{\bar{i}4}\delta_{j3} + \frac{1}{\sqrt{3}}\delta_{\bar{i}6}\delta_{j1}, \quad (\text{E18})$$

$$\mathcal{P}_{ij}^{\Xi^{*-}} = \sqrt{\frac{2}{3}}\delta_{\bar{i}5}\delta_{j3} + \frac{1}{\sqrt{3}}\delta_{\bar{i}6}\delta_{j2}, \quad (\text{E19})$$

$$\mathcal{P}_{ij}^{\Omega^-} = \delta_{\bar{i}6}\delta_{j3}. \quad (\text{E20})$$

In this sector, the axial diquarks belong to the sextet representation of $SU_f(3) \times SU_f(3)$. Therefore, the index \bar{i} runs from 1, ..., 6 representing the diquarks (uu) , (ud) , (dd) , (us) , (ds) , and (ss) , respectively.

All the projectors satisfy explicitly Eqs. (E1) and (E2).

APPENDIX F: QUARK-DIQUARK POLARIZATION FUNCTION

We will detail here the reduction of the quark-scalar diquark polarization function in Eq. (67). At finite temperature, the polarization function (67) reads

$$\Pi_{k\bar{k}}(i\nu_l, \mathbf{p}) = T \sum_n \int \frac{d^3q}{(2\pi)^3} S_k(i\nu_l - i\omega_n, \mathbf{p} - \mathbf{q}) t_{\bar{k}}(i\omega_n, \mathbf{q}), \quad (\text{F1})$$

where $i\nu_l$ is a fermionic Matsubara frequency which will be analytically continued to real values at the end of the calculation. The variable $i\omega_n$ is a bosonic Matsubara frequency appearing in the diquark propagator in the pole approximation (52),

$$\Pi_{k\bar{k}}(i\nu_l, \mathbf{P}) = -T g_{[qq] \rightarrow qq}^2 \sum_n \int \frac{d^3q}{(2\pi)^3} \frac{1}{(i\omega_n + \epsilon_{\bar{k},q})(i\omega_n - \epsilon_{\bar{k},q})} \frac{(P_0 - i\omega_n)\gamma_0 + m_k \mathbb{I}}{(i\omega_n - P_0 + E_{k,q})(i\omega_n - P_0 - E_{k,q})}, \quad (\text{F2})$$

with $\epsilon_{\bar{k},q}^2 = m_{\text{DIQ},\bar{k}}^2 + \mathbf{q}^2$ and $E_{k,q}^2 = m_k^2 + (\mathbf{P} - \mathbf{q})^2$ (note that k represents the quark flavor, not a momentum).

The Matsubara summation is performed taking into account the four poles using standard techniques [35]. We can express the final result in terms of four functions (one coming from each pole):

$$\Pi_{k\bar{k}}(P_0, \mathbf{P} = 0) = -\frac{g_{[qq] \rightarrow qq}^2}{8\pi^2} (J_+^F + J_-^F + J_+^B + J_-^B), \quad (\text{F3})$$

where we have considered the baryon at rest $\mathbf{P} = 0$ and performed the analytical continuation $i\nu_l \rightarrow P_0 + i\epsilon$. We have also defined four J functions, whose real and imaginary parts are given by

$$\text{Re}J_{\pm}^F = \frac{1}{2P_0} \text{P.V.} \int_{m_k}^{\Lambda_E} dE_{k,q} [1 - 2n_F(\pm E_{k,q})] (\mathbb{I}m_k \mp \gamma_0 E_{k,q}) \frac{\sqrt{E_{k,q}^2 - m_k^2}}{E_{k,q} - E_{\pm}}, \quad (\text{F4})$$

$$\text{Im}J_{\pm}^F = \frac{\pi}{2P_0} (\mathbb{I}m_k \mp \gamma_0 E_{\pm}) \sqrt{(E_{\pm})^2 - m_k^2} [1 - 2n_F(\pm E_{\pm})] \Theta(\Lambda_E - E_{\pm}) \Theta(E_{\pm} - m_k), \quad (\text{F5})$$

$$\text{Re}J_{\pm}^B = \frac{1}{2P_0} \text{P.V.} \int_{m_{\text{DIQ},\bar{k}}}^{\Lambda_{E^*}} d\epsilon_k [1 + 2n_B(\epsilon_k)] [\mp \mathbb{I}m_k + \gamma_0(\epsilon_k \mp P_0)] \frac{\sqrt{\epsilon_k^2 - m_{\text{DIQ},\bar{k}}^2}}{\epsilon_k - \epsilon_{\pm}}, \quad (\text{F6})$$

$$\text{Im}J_{\pm}^B = \frac{\pi}{2P_0} [\mp \mathbb{I}m_k + \gamma_0(\epsilon_{\pm} \mp P_0)] \sqrt{(\epsilon_{\pm})^2 - m_{\text{DIQ},\bar{k}}^2} [1 + 2n_B(\epsilon_{\pm})] \Theta(\Lambda_{E^*} - \epsilon_{\pm}) \Theta(\epsilon_{\pm} - m_{\text{DIQ},\bar{k}}), \quad (\text{F7})$$

with $\Lambda_E = \sqrt{\Lambda^2 + m_k^2}$, $\Lambda_{E^*} = \sqrt{\Lambda^2 + m_{\text{DIQ},\bar{k}}^2}$. In addition,

$$E_{\pm} = \pm \frac{m_{\text{DIQ},\bar{k}}^2 - m_k^2 - P_0^2}{2P_0}, \quad (\text{F8})$$

$$\epsilon_{\pm} = \mp \frac{m_{\text{DIQ},\bar{k}}^2 - m_k^2 + P_0^2}{2P_0}, \quad (\text{F9})$$

and the Fermi and Bose functions $n_F(E_k) = (e^{E_k/T} + 1)^{-1}$, $n_B(\epsilon_k) = (e^{\epsilon_k/T} - 1)^{-1}$.

The axial diquark case—which we have omitted for simplicity—is straightforward. This case differs in the explicit appearance of Dirac indices in Eq. (67). In addition, note that Eq. (67) carries an opposite sign to Eq. (69), but this cancels with the different sign in the diquark propagators [cf. Eqs. (52) and (54)]. We have neglected the term proportional to $p^\mu p^\nu$ in Eq. (54), which is suppressed by the diquark mass squared.

-
- [1] Y. Aoki, G. Endrodi, Z. Fodor, S. D. Katz, and K. K. Szabo, *Nature (London)* **443**, 675 (2006).
[2] P. Braun-Munzinger, J. Stachel, J. P. Wessels, and N. Xu, *Phys. Lett. B* **344**, 43 (1995).
[3] A. Andronic, P. Braun-Munzinger, and J. Stachel, *Nucl. Phys. A* **772**, 167 (2006).
[4] R. Preghenella (ALICE Collaboration), *Acta Phys. Polon. B* **43**, 555 (2012).
[5] A. Bazavov, T. Bhattacharya, M. Cheng, C. DeTar, H. T. Ding, S. Gottlieb, R. Gupta and P. Hegde *et al.*, *Phys. Rev. D* **85**, 054503 (2012).
[6] S. Chatterjee, R. M. Godbole, and S. Gupta, *Phys. Lett. B* **727**, 554 (2013).
[7] S. Chatterjee and B. Mohanty, *Phys. Rev. C* **90**, 034908 (2014).
[8] S. Chatterjee, B. Mohanty, and R. Singh, [arXiv:1411.1718](https://arxiv.org/abs/1411.1718).
[9] R. Bellwied, S. Borsanyi, Z. Fodor, S. D. Katz, and C. Ratti, *Phys. Rev. Lett.* **111**, 202302 (2013).
[10] S. P. Klevansky, *Rev. Mod. Phys.* **64**, 649 (1992).
[11] M. Buballa, *Phys. Rept.* **407**, 205 (2005).
[12] D. Lehmann, Ph.D. thesis, Erlangen Universität, 1996.
[13] A. Buck, R. Alkofer, and H. Reinhardt, *Phys. Lett. B* **286**, 29 (1992).
[14] U. Vogl and W. Weise, *Prog. Part. Nucl. Phys.* **27**, 195 (1991).
[15] Y. Nambu and G. Jona-Lasinio, *Phys. Rev.* **122**, 345 (1961).
[16] T. Hatsuda and T. Kunihiro, *Phys. Rept.* **247**, 221 (1994).
[17] C. Ratti, M. A. Thaler, and W. Weise, *Phys. Rev. D* **73**, 014019 (2006).
[18] B. J. Schaefer, J. M. Pawłowski, and J. Wambach, *Phys. Rev. D* **76**, 074023 (2007).
[19] H. Hansen, W. M. Alberico, A. Beraudo, A. Molinari, M. Nardi, and C. Ratti, *Phys. Rev. D* **75**, 065004 (2007).
[20] G. Goessens, Ph.D. thesis, Université de Lyon, 2012.
[21] E. Blanquiere, *J. Phys. G* **38**, 105003 (2011).

- [22] P. Rehberg, S. P. Klevansky, and J. Hufner, *Phys. Rev. C* **53**, 410 (1996).
- [23] C.-f. Mu, Y. Jiang, P.-f. Zhuang, and Y.-x. Liu, *Phys. Rev. D* **85**, 014033 (2012).
- [24] J. Beringer *et al.* (Particle Data Group Collaboration), *Phys. Rev. D* **86**, 010001 (2012).
- [25] B. B. Abelev *et al.* (ALICE Collaboration), *Phys. Rev. C* **91**, 024609 (2015).
- [26] H. Reinhardt, “Effective Hadron Theory of QCD,” Egyptian-German Spring School and Conference (Forschungszentrum Jülich GmbH, Jülich, Germany, 1992).
- [27] S. P. Klevansky and R. H. Lemmer, [arXiv:hep-ph/9707206](https://arxiv.org/abs/hep-ph/9707206).
- [28] N. Ishii, W. Bentz, and K. Yazaki, *Nucl. Phys. A* **587**, 617 (1995).
- [29] F. Gastineau and J. Aichelin, *J. Phys. G* **28**, 2017 (2002).
- [30] F. Gastineau, Ph.D. thesis, Université de Nantes, 2002.
- [31] E. Blanquier, Ph.D. thesis, Université de Toulouse, 2013.
- [32] M. Fierz, *Z. Phys.* **104**, 553 (1937).
- [33] R. Alkofer and H. Reinhardt, *Chiral Quark Dynamics*, Lecture Notes in Physics (Springer, Berlin, 1995).
- [34] P. Rehberg and S. P. Klevansky, *Annals Phys.* **252**, 422 (1996).
- [35] J. I. Kapusta and C. Gale, *Finite-Temperature Field Theory: Principles and Applications* (Cambridge University Press, Cambridge, 2006).
- [36] G. D. Mahan, *Many-Particle Physics* (Springer, Berlin, 2000).
- [37] G. Sun, L. He, and P. Zhuang, *Phys. Rev. D* **75**, 096004 (2007).
- [38] M. Oettel, Ph.D. thesis, Tübingen Universität, 2000.
- [39] D. B. Lichtenberg and L. J. Tassie, *Phys. Rev.* **155**, 1601 (1967).
- [40] C. Hanhart and S. Krewald, *Phys. Lett. B* **344**, 55 (1995).